ABSTRACT

Title of Thesis: WARM SEASON HYDROLOGIC PROCESSES IN A BOREAL FOREST HILLSLOPE AND CATCHMENT, NEWFOUNDLAND

Haley Talbot-Wendlandt
Master of Science
2020

Thesis directed by: Dr. Karen Prestegaard
Associate Professor
Department of Geology

Prior investigations into boreal forest ecosystems have examined hydrological processes on plot scales, examining factors such as precipitation, soil characteristics, tree rooting depths, evapotranspiration, infiltration, and groundwater, or on the catchment scale, investigating factors such as stream discharge and water chemistry. In this study, I examine hydrological processes at both plot and catchment scales, with the goal of understanding how rooting depths influence evapotranspiration (ET) and the effects of ET on catchment discharge and water chemistry. Evapotranspiration was found to influence seasonal and diurnal fluctuations in groundwater table, stream discharge, and stream electrical conductivity. Tree rooting depths were shallow, primarily within O and Ae soil horizons, suggesting that these trees intercept infiltrating water, reducing summer groundwater recharge. Stream electrical conductivity increased with cumulative ET. Summer streamflow minima coincided with hillslope groundwater minima. Stream depth and conductivity exhibited similar diurnal patterns, suggesting variations in groundwater contributions and opportunities for future research.

WARM SEASON HYDROLOGIC PROCESSES IN A BOREAL FOREST HILLSLOPE AND CATCHMENT, NEWFOUNDLAND

by

Haley Talbot-Wendlandt

Thesis submitted to the Faculty of the Graduate School of the
University of Maryland, College Park, in partial fulfillment
of the requirements for the degree of
Master of Science
2020

Advisory Committee:
Professor Karen Prestegaard, Chair
Professor Michael Evans
Professor Sujay Kaushal
Professor Susan Ziegler

Acknowledgements

Thanks to GSA for granting funding to support this research, the NL-BELT study site system for the infrastructure support and extensive data, and the Canadian forest service for allowing us use of their field station. Additional thanks to my advisor, Karen Prestegaard; to our Newfoundland field collaborators, Susan Ziegler, Zachary Gates, and Christian Gaviria; and to our other collaborators, Samantha Volz, Devin Simmons, and Dilanka Athukorala.

Table of Contents

List of Tables

List of Figures

Chapter 1: Introduction and Scope

Background and Previous Work

Earth has three major forests biomes (boreal, temperate, and tropical), which are distributed by latitude (light and growing season length) and rainfall distribution (Ulrich et al. 2016). These different forests have significantly different canopy characteristics, root structures, and soil characteristics (Jackson et al. 1996; Ulrich et al. 2016; Fan et al. 2019) that influence the storage of carbon in biomass or soils. Boreal forest soils are important carbon sinks, storing large amounts of soil organic carbon and mineral carbon (e.g. Angstmann et al. 2012; Scharlemann et al. 2014), which affects global climate regulation. Understanding how these forests and associated soils will respond to climate change requires that we understand the connections among climate, forest productivity, hydrological processes, and soil characteristics. Prior research at maritime boreal sites along a north-south climate gradient has indicated that soil organic carbon (SOC) stocks currently remain constant as net ecosystem production replaces SOC lost via decomposition and dissolved organic carbon (DOC) fluxes (Ziegler et al. 2017). High soil water content near the surface can limit organic matter decomposition, but movement of water through organic layers can transport carbon to the atmosphere via respiration (CO_2, CH_4), to adjacent aquatic systems, or to mineral soil storage by transforming carbon to solid phases (Ziegler et al. 2017; Bowering et al. 2020). Water fluxes can remove carbon from carbon-rich soils in dissolved or particulate forms (DOC or POC); mobilized carbon can then be transferred laterally to aquatic systems or infiltrated vertically into soils where carbon can be stored in aggregates or on mineral surfaces (Lehmann and Kleber 2015).

Global warming is predicted to lead to a warmer and slightly wetter climate in the boreal region of Atlantic Canada (Wang et al. 2014). The effects of these changes on boreal forest transpiration, productivity, and soil carbon storage are not yet defined. Lengthening of growing seasons may lead to higher forest productivity; however, higher transpiration and warmer temperatures may lead to water limitations, which could limit carbon storage (D'Orangeville et al. 2018). Furthermore, increases in precipitation could increase carbon transport. Water fluxes in soils are sensitive to climate via evapotranspiration (ET), the duration of snow cover, and the precipitation-ET difference, which can seasonally adjust water tables and affect fluxes to first order streams. Water below the rooting depth of plants is not available for ET, and it recharges local groundwater and contributes to stream baseflow. Groundwater can move laterally towards lower elevation regions (e.g. riparian zones) where it can again be available for ET. Therefore, rooting depths in hillslopes and riparian zones can affect the distribution of groundwater levels in landscapes (Fan et al. 2017). In forested regions, hillslope eco-hydrological processes likely govern variations in streamflow from catchments; therefore, the effects of seasonal variations in processes should be evaluated at both hillslope and catchment scales. Climate change in boreal regions will likely affect the timing and amount of snowmelt (Pulliainen et al. 2017), and also the timing and amount of evapotranspiration. Changes in evapotranspiration will affect biomass production, groundwater levels, streamflow, and soil carbon storage. The interactions among evapotranspiration, soil characteristics, and hydrological processes have not been examined in maritime boreal forests and are thus the focus of this investigation.

Forest vegetation exerts significant controls on hydrological processes; trees transport water via transpiration from roots in the soil into the atmosphere through stomata in leaves (e.g. Reich et al. 2018). In most forested regions evapotranspiration is the major water loss term in annual water balances; however, boreal forests have short growing seasons, which reduces annual ET compared to temperate forests (Trenberth et al. 2007, Brantley et al. 2017). Trees and their roots are continually modifying the soils in which they grow via additions of organic carbon through leaf litter and root contributions, enhanced chemical weathering by root exudates and physical weathering by roots, and enhanced soil stresses that increase soil and saprolite hydraulic conductivity (Brantley et al. 2017; Billings et al. 2018). ET links tree and soil characteristics directly to the hydrological cycle.

Plants have adapted to a wide range of moisture conditions including seasonal dryness and shallow or deep groundwater tables. Many tree species experience root rot with shallow groundwater depths, while extending deep roots to take advantage of deep groundwater. Trees generally concentrate their root growth at the shallowest depth where water is readily available (Brantley et al. 2017; Fan et al. 2017). Water availability is reliant on the balance of water fluxes and therefore the amount and timing of precipitation and ET. Observational data displays a strong correlation between rooting depth and water table depth (Fan et al. 2017). However, correlation is not evidence of causation: rooting depths and associated ET also cause water table declines, water tables are seasonally variable (not static), and some tree roots can extend far below average and even minimum water tables (Pierret et al. 2016). Most studies of rooting depths do not include all roots, often using data sets where excavations of deep tree roots were

"terminated at arbitrary depths" (Pierret and Lacombe 2018). Researchers have also suggested that because ET removes stored water, groundwater depth may be a consequence, not a cause of, rooting depth (Pierret et al. 2016). Increases in temperature caused by global warming may increase maximum daily ET demands, extend growing seasons, or both. These changes in seasonal ET could affect water availability, water table depth, and the suitability of existing and invading tree species to the changed environment. Although identification of rooting depth and water table depth preferences (or limitations) for tree species may be simplistic, this may provide an initial approximation for identifying hydrological ranges of species and how they might respond to climate change. Understanding the details, however, requires an examination of the interactions among plant transpirative demand, soil characteristics, ET, and water table depth in climate-sensitive biomes.

The approach of this research is to evaluate the water balance and interactions between biological and physical hydrological processes at both the catchment and hillslope scales. Water balances quantify the fate of precipitation (PPT) through storage and losses due to runoff and evapotranspiration: $PPT = ET + Runoff + \Delta Storage$ (Figure 1). At the hillslope or plot scale, precipitation and groundwater data can be directly measured to quantify change in storage ($\Delta Storage$), runoff is calculated from groundwater data, and ET is estimated from other parameters. At the catchment scale, streamflow runoff (a catchment-integrated quantity) is quantified, but change in groundwater storage is estimated from other water balance components (Figure 1). Seasonal variations in temperature and evapotranspirative demand can drive seasonality in groundwater table minima. Water table minima can result from groundwater drainage

without recovery, or from rates of groundwater withdrawal via ET that are greater than precipitation rates.

Scope of Study

This study examines boreal forest warm season hydrological processes at the hillslope and catchment scales. In this study, I integrate data on tree rooting depth, soil characteristics, groundwater depth, and ET estimates at the hillslope scale; and I use stream depth/discharge, ET estimates, and stream conductivity to evaluate hydrologic processes at the catchment scale. The thesis presents this research in two results chapters. Chapter 2 includes the results of field and modeling studies on the hillslope scale, quantifying the water balance by using field-based instrumentation to measure PPT, ET, and groundwater (Figure 2). Field data on tree rooting depths and their relationship to soil characteristics, groundwater levels, and ET were evaluated to identify likely sources of water for tree transpiration. Chapter 3 focuses on hydrological processes at the catchment scale; in this chapter, I link the timing of annual streamflow minima with hillslope groundwater minima. I examine the cause of observed steady increases in stream electrical conductivity by comparing conductivity with cumulative hillslope ET. I also identify strong diurnal patterns in both stream discharge and conductivity. I evaluate the timing of the coincident streamflow and electrical conductivity maxima to determine whether these variations indicate diurnal changes in streamwater sources. The thesis concludes with a discussion of the overall results and implications of this research.

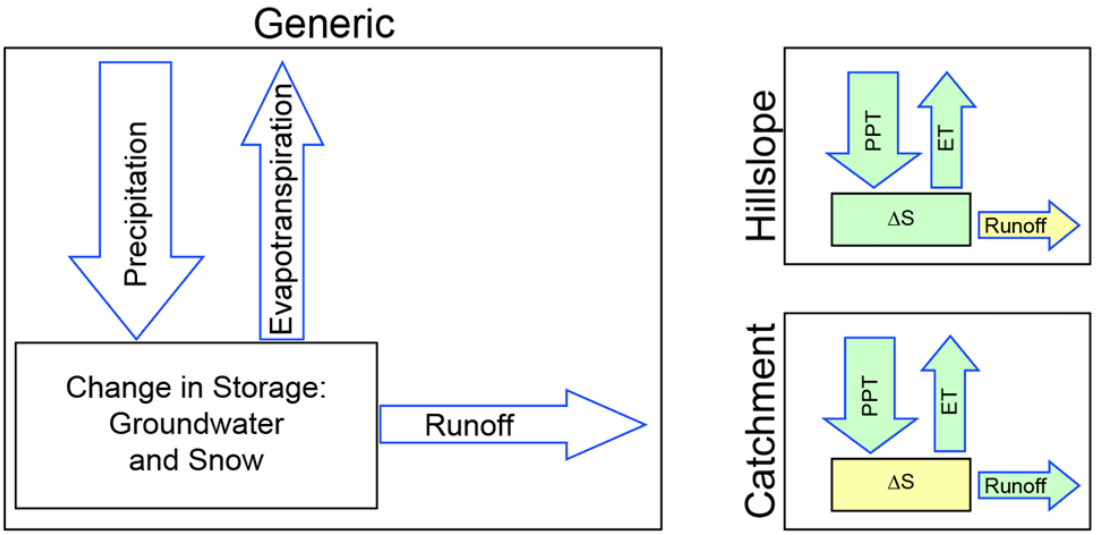

Figure 1. On the left, a diagram of a generic water balance: ΔStorage (GW + snow) = PPT – ET – Runoff. On the right, examples of what is measured (in green) versus what is calculated based on measurements (in yellow) in hillslope and catchment water balances.

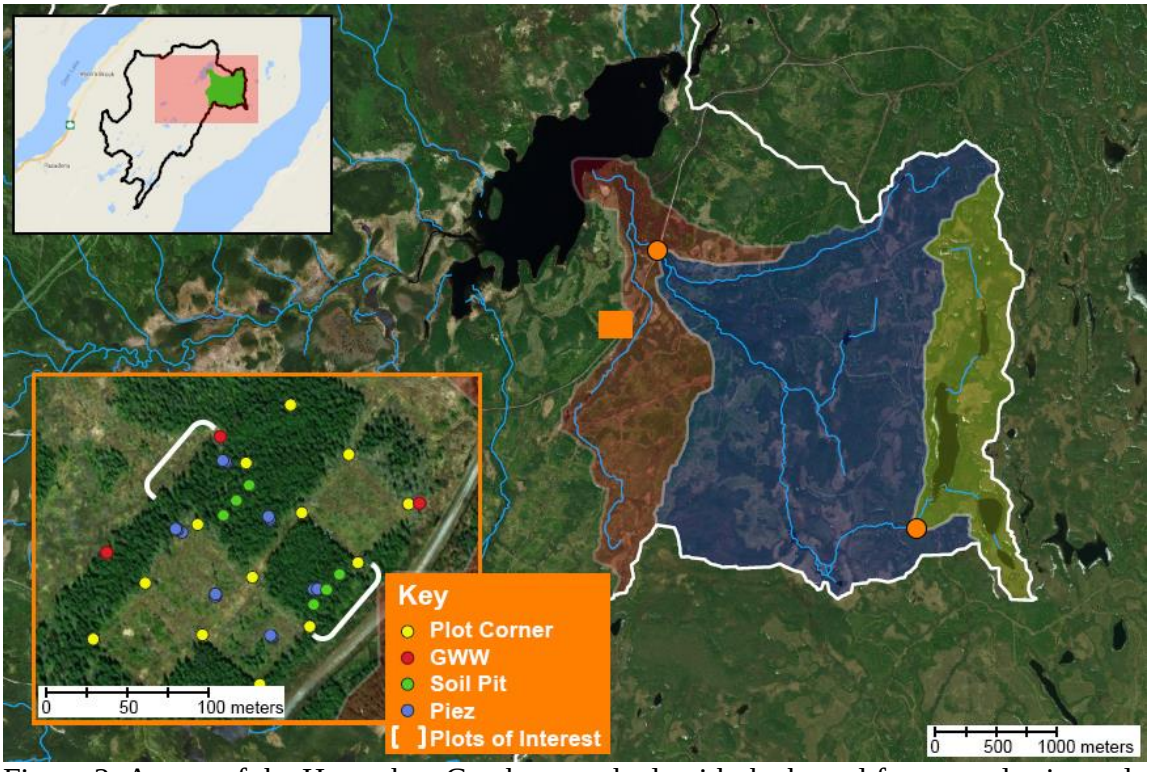

Figure 2. A map of the Horseshoe Creek watershed, with the boreal forest study site and instrumentation highlighted. Stream gauges are marked by orange points, the yellow overlay denotes the upper catchment, and the blue overlay denotes the lower catchment. For the hillslope plot, GWW = groundwater well and Piez = piezometer. The studied hillslope area for this investigation is enclosed by the white brackets. The hillslope slopes from the southeast to the northwest. Modified from Meyers-Pigg et al., 2018.

Chapter 2: Linking Soil Characteristics, Rooting Depths, Evapotranspiration, and Groundwater Depths in a Boreal Forest Hillslope, Horseshoe Creek, Newfoundland

Introduction

Boreal forest soils are important carbon sinks, storing carbon in organic and mineral soil horizons (Angstmann et al. 2012; Scharlemann et al. 2014; Ziegler et al. 2017). These carbon stores may be sensitive to global climate change: warming and extension of the growing season may increase primary productivity, which may increase carbon storage. Increases in warm season evapotranspiration may lead to increased depth or duration of soil drying, which may lead to increased oxidation of organic matter or higher likelihood of forest fires (D'Orangeville et al. 2018). Drying of surface soils may push root development to greater depths, which may lead to storage of organic matter (Pierret et al. 2016). A wetter boreal climate would likely lead to higher rates of water fluxes through organic horizons and removal of organic carbon in dissolved phases (Tranvik et al. 2009, Senar et al. 2018). Therefore, research on relationships among soil characteristics, rooting depths, ET, and groundwater levels is important to understand how these processes might change in a warmer, wetter climate. Prior research in the boreal forests of Atlantic Canada with plots established along a north-south climate gradient indicate a southerly increase in ET and associated biomass productivity (Ziegler et al. 2017). This association among ET, productivity, and carbon storage may be responsible for the observation that currently SOC stocks are not changing, suggesting that net ecosystem production replaces SOC lost via decomposition and dissolved organic carbon fluxes (Ziegler et al. 2017). High soil water content near the surface can limit

organic matter decomposition, but water movement through these shallow horizons can facilitate carbon loss to the atmosphere via respiration, to adjacent aquatic systems, or to mineral soil storage via vertical infiltration and sorption (Tranvik et al. 2009; Bowering et al. 2020). Recent research indicates that water fluxes can remove carbon as DOC from carbon-rich boreal soils; soil water flow can then transfer this mobilized DOC laterally to aquatic systems or infiltrate it vertically into soils where the carbon can be stored in aggregates or on mineral surfaces (Lehmann and Kleber 2015). In wet boreal climates, the spring and fall periods that occur prior to and after the ET season can be times of high soil water content and significant soil water and carbon fluxes. Bowering et al. (2020) showed that the DOC concentration in soil water is high in the fall. Precipitation as rainfall after transpiration shutdown can cause an increase in soil water and carbon fluxes (Bowering et al. 2020). This suggests that the amount and seasonal duration of ET can influence biomass production and carbon storage, and cessation of ET can trigger time intervals of significant DOC fluxes.

Boreal forests are located in high latitudes and therefore have short growing seasons, which provide seasonal limits on ET rates (Angstmann et al. 2012). Both temperature and light limitations of boreal transpiration can affect annual ET and biomass production.

The relationship between rooting depths and ET demand has not been examined in detail in eastern Canadian maritime boreal forests, but the presence of a shallow water table suggests shallow rooting depths (Fan et al. 2017, 2019). Evapotranspiration then moves that shallow water vertically into the atmosphere, decreasing soil moisture and lowering groundwater tables. Therefore, determining seasonal and annual water balances

and how they are affected by and influence soil properties, ET, and plant rooting depths will improve our understanding of hydrological processes in this environment and contribute to an understanding how these boreal forest ecosystems and associated carbon storage reservoirs will respond to climate change.

Although ET is difficult to measure directly, consequences of transpiration can be observed as changes in soil and groundwater. ET demand can cause large seasonal fluctuations in groundwater storage. This seasonal variation is not always characterized in studies that link groundwater level to rooting depth or other phenomena (e.g. Fan et al. 2017). That is one reason why this study aims to develop a method of accurately and succinctly representing the depth of the groundwater table, without over-simplifying it to an annual average.

Previous work indicates that although precipitation in the maritime boreal forest is not seasonal, groundwater exhibits two annual minima: a) during winter when precipitation is stored as snow, which insulates the soil, limiting groundwater recharge but maintaining groundwater drainage through the unfrozen soil; and b) during late summer as cumulative ET demand utilizes available water stocks. However, it is unclear whether trees influence the summer groundwater level by directly extracting groundwater, or by intercepting precipitation and preventing groundwater recharge. In general, shallow roots are grown to intercept rainwater and soil water flows (throughflow), whereas deep roots allow trees to obtain nutrients and groundwater that are more difficult to access but are often more reliable (Pierret et al. 2016). Trees generally grow roots only to the depth required to reliably obtain water and nutrients, as deeper roots are more energy-intensive to grow (Brantley et al. 2017). Tree rooting depth

appears to be closely linked with tree species and depth to water table, with boreal genera such as *Picea* having relatively shallow (mean = 0.74 m) rooting depths across compiled data (Fan et al. 2017). Therefore, investigating the tree rooting depth and root structure in relationship to the groundwater table and ET demand could be used to identify where the trees draw their water.

Hypotheses:

H1: *Picea mariana* (black spruce) trees in the wet boreal forests of western Newfoundland can receive most of their water requirements from infiltrating water, and therefore they have very shallow root systems.

H2: Seasonal variations in groundwater levels can be predicted from the water balance:

ΔGW storage = PPT-ET $\pm$ Drainage. The local water balance generates groundwater minima in late summer and variations in groundwater depth between upslope and downslope positions.

H3: Root density distributions will be inversely correlated with summer groundwater level probability distributions.

Study Site and Methods

Horseshoe Creek Study Site

The boreal forest field site is Horseshoe Creek watershed in Newfoundland, Canada (Figure 2), a 13.34 km^2 catchment that is also an experimental watershed for the Newfoundland-Labrador Boreal Ecosystem Latitudinal Transect (NL-BELT) study sites,

which were selected to encompass a 500 mm southerly increase in mean annual precipitation and a 5.2°C increase in mean annual temperature over 6° latitude. The Horseshoe Creek study area includes forested and harvested plots instrumented with groundwater wells, piezometers, and throughflow pits; and two stream gauges that monitor stage, temperature, and conductivity. The study plots are located on a straight hillslope with minimal curvature (Figure 2). Harvested plots were clear-cut in 2003 and have since been left to recover (Moroni et al. 2009). Wells were placed in upslope and downslope locations in both forested and harvested plots. Piezometers were aligned to give upslope, midslope, and downslope replicates in forested and harvested transects.

Vegetation on the forested hillslope study plot is dominated by black spruce (*Picea mariana*) and mosses (Moroni et al. 2009). The site has a shallow water table depth, mean annual precipitation 1095 mm, and mean annual temperature 3.6°C. The precipitation is non-seasonal, but ET demand (475 mm annually, 43% of MAP) and snow storage fluctuate throughout the year based on light availability and air temperature. Other characteristics of the site are listed in Table 1. The rooting depth for the *Picea*-dominated forest is expected to be shallow, but this species based estimate is not well-constrained, as is shown in Figure 3 (Fan et al. 2017).

Field Data Collection

Data for this investigation was obtained from field surveys, soil pits, and hydrological monitoring equipment installed on the field site in Horseshoe catchment (Figure 4). Piezometers and wells were previously installed at upslope and downslope positions at the field site. Field characterization of vegetation and the establishment of

soil pits to collect soil and root characteristics were conducted in August 2019. These field procedures included the following: a) vegetation characterization (moss depths, tree diameter, tree density) at the upslope and downslope positions; and b) soil characterization (bulk density, water content, root content).

The soil pit data relies primarily on using on-site measurements to characterize vegetation, root, and soil properties. As the focus is on forest processes, and in order to account for the influence of hillslope processes like lateral flow, all the soil pits were dug in the completely-forested plots (white-bracketed area, Figure 2), with 3 pits upslope and 3 downslope in order to give 3 replicates of each. The upslope and downslope pits were situated along two transects perpendicular to the hillslope, and the pits were evenly spaced so that each upslope pit was aligned with a downslope pit along a transect parallel to the hillslope, resulting in a 2x3 grid of soil pits.

During the field season in August 2019, I was primarily responsible for collecting and analyzing tree diameter, tree density, rooting depth, and root size (length, diameter, and volume) data. Root data and soil samples were obtained from soil pits that were dug by a combined University of Maryland and Memorial University of Newfoundland research team. I will use soil properties obtained from these samples along with hydrological data from the experimental field site and other sources to evaluate soil-root relationships and root-hydrology relationships. Below I describe the field data that were collected in August 2019.

1. Tree surveys:

Tree properties (species, tree diameter, tree cross-sectional area) were determined by identifying each tree to the species level and measuring the chest-high diameter of

each tree within six 7 x 7 m plots at the Newfoundland site, each centered on a sampled soil pit. These data were used to evaluate overall tree density of each plot (in m^2/m^2), species composition, and species richness.

2. Microtopography and moss thickness:

Changes in topography and moss thickness were measured by taking transects across the hillslope, parallel to the soil pit transects. The transects were created by setting a level reference line approximately 1 meter above the ground surface, then walking along the line and stopping every 0.25 meters to take a measurement of the distance from the ground surface to the reference line. Moss and organic horizon thicknesses were measured by cutting a slit in the moss carpet using a soil knife, then opening it to measure the thickness of the live moss, dead moss, and organic horizons. As measuring the moss thickness was slightly more invasive than the topographic measurements, thickness measurements were taken every 1 meter. Microtopography and thickness transects were adjacent and parallel to the soil pit transects, described below.

3. Soil sampling and analyses:

Two transects were laid out perpendicular to the hillslope, one upslope and one downslope, and 3 soil pits were dug along each transect. Vertical soil profiles were obtained from soil pits and used to obtain samples for soil and root characteristics. Each vertical soil profile was measured by digging a soil pit 1 x 1 m in footprint and approximately 0.7 to 1 m deep (or as far as was needed to reach the base of the C horizon or water table). Pictures of these pits are shown in Figure 4. Soil sampling was conducted by horizon. Two samples were taken from each horizon and were analyzed for bulk density and moisture content by Zachary Gates of Memorial University of

Newfoundland. Samples of known volume were weighed, then air-dried (for at least 1.5 weeks), oven-dried (at 40 °C for 6-12 hours), and reweighed to calculate moisture content.

4. Root sampling, measurement, and analysis:

Procedures for root analysis were developed in Newfoundland to obtain samples directly from the 1 m^2 excavated soil pits. Although this method was labor-intensive and it was difficult to obtain fine root samples (Maeght et al. 2013), it provided a direct measurement of the volume of roots per soil horizon. The entire 1 x 1 m area of the pit was used to sample large roots (≥0.1 cm diameter) over the horizon interval. Due to the large number of small roots, three 20 x 20 cm subsamples were collected in each soil horizon to sample medium-to-fine roots (<0.1 cm diameter). The volume of these roots was then normalized to the entire soil horizon. Roots finer than 0.1 cm diameter broke too easily to separate from the soil matrix (Figure 4, bottom right).

All the root samples were weighed, dried (at approximately 60°C for at least 8 hours), and reweighed; and for large roots, we measured the length and diameter of each root in order to determine root weight per unit volume, which could then be applied to the small root weights in order to determine total root volume.

Groundwater Monitoring

Groundwater table elevation data have been acquired using HOBO water level loggers which were placed in 3-meter deep wells and maintained for about 4 years. Well 8 is located downslope of the soil pits and was the source of downslope water table data. Figure 6 shows most of the WY 2018 annual cycle at this location. 1-meter deep

piezometers were also placed throughout the study site; piezometer 5 is located upslope of the soil pits and was the source of upslope water table data. Precipitation data is available for the site from local project data and NASA global satellite observations.

Analysis of Hydrological Data

1. Evaluation of ET from MODIS data

8-day ET estimates were calculated for the period 2010-2013 by Devin Simmons using data from NASA's MODIS16 satellite (Simmons 2019). Simmons compared estimates of ET based on MODIS data with flux tower measurements of ET at sites located throughout boreal forests in Canada. He found that there is strong agreement (R^2 = 0.77 to 0.89) between flux towers and the MODIS calculations, indicating that the MODIS calculations are a relatively accurate estimate of ET. These MODIS calculations were performed on a spatial scale of 9 km^2 plots.

2. Calculation of hillslope water balance to obtain changes in GW storage

I created a simple model for seasonal change in groundwater storage based on the water balance method of groundwater determination. The water balance method assumes that the change in water storage is equal to the input of precipitation minus the outputs of ET and runoff (Figure 1). The "catchment" model was used to calculate a simple change in groundwater storage for the hillslope study site by using $\Delta GW = PPT-ET$, assuming no storage as snow and no runoff or drainage.

First, average precipitation and evapotranspiration were calculated for 8-day periods over multiple years (2010-2014 for ET, 2016-2019 for PPT). These years were selected because they were the most recent years with good-quality data available; MODIS data is not yet available for recent years, and precipitation data was directly

measured at the site starting in 2016. Multiple years were averaged in order to minimize variability caused by using different time periods for the ET data and PPT data. This is likely fair because ET demand is dependent on factors such as amount of incoming radiation and vegetation density which have little variation from year to year, and MODIS calculations are for a large spatial scale (9 km^2, compared to the 0.01 km^2 hillslope plot). However, as precipitation data is only available for 4 years, a large storm during one year can create a peak for that timeframe. I calculated a simple estimate of change in hillslope groundwater storage over time by subtracting ET demand from the precipitation input. This model of groundwater storage is intended to represent the hillslope as a whole, as there is lateral flow from the top of the hillslope to the bottom which this calculation does not incorporate.

3. Conversion of changes in GW storage to changes in GW level

Water balance considerations evaluate the change in groundwater storage. To model the corresponding change in groundwater table elevation, groundwater drainage and specific yield (proportion of total soil volume occupied by water that is not tightly held and can be released from the soil) were incorporated into the water balance equation: $\Delta GW = (PPT - ET)*SY - Drainage$.

In a first approximation, I used a specific yield of 0.44 and a constant 8-day drainage loss of 2.4 cm. This specific yield was obtained from measured specific yields for peaty soil (Morris and Johnson 1967). Peat-like soil is a reasonable assumption for the first 15 cm below the ground surface, which is rich in moss and organic materials. The predicted groundwater table, which is modeled for the downslope site, only drops under 15 cm below the surface for 3.5 months, from mid-June to late October. In addition, lower soil

layers have lower hydraulic conductivity (Bowering et al. 2020) and similarly high porosity (Table 2) compared to the organic horizon, so although the assumption of a peaty soil does not hold and the 0.44 specific yield value is likely not appropriate, the top of the water table only occupies this space for a short period of time. The 8-day drainage was calculated based on measured 1-day infiltration of 3 mm, which was multiplied to match the 8-day period of ET and precipitation.

4. Seasonal separation of time series and identification of seasonal minima

Groundwater minima were visually identified on a plot of the WY 2018 data, then confirmed in the raw data by finding the minimum value within a certain time range. Seasons were demarcated to align with changes in groundwater behavior (visible in Figure 5): "winter" (12/1-2/28) is when groundwater levels rise and fall in sudden, relatively symmetrical pulses; "snowmelt" (3/1-5/31) is when the rises and falls become more rounded; "ET" (6/1-9/30) is the time period where there is a diurnal pattern of a sharp decrease in groundwater level during the day and a more slight decrease overnight; and "fall" (10/1-11/30) is when the water table rises in sudden pulses and falls more gradually, creating an asymmetrical pattern of rise and fall.

5. Groundwater depth exceedance probability distributions

As the groundwater level varies on the daily timescale and on seasonal timescales, listing the average or mean groundwater level would not accurately represent the pattern of groundwater variation. Therefore, groundwater depth probability distributions were developed for the top and bottom of the hillslope for WY 2018 (Figure 6). These distributions were created by dividing data into seasons (as described above), then calculating the cumulative percent of the season that each depth is saturated. The

resulting graph shows the percent of time that the top of the water table is at or above the given depth, making it possible to determine how frequently the different soil horizons are saturated.

Results

Tree and Moss Characteristics

Trees are prevalent at the site, and they are relatively uniform in trunk size (Figure 7), with 91% of trees having a diameter between 2.5 cm and 17.5 cm. Their thin trunks and wide spacing result in a low tree density, ranging from 0.0069 to 0.0088 m^2/m^2 at the measured plots (Table 2). The cumulative tree area covers less than 1% of the ground area. Furthermore, tree trunk size and tree density did not vary significantly among the sites of the 6 soil pits or between the upslope and downslope transects, therefore, soil characteristics were measured at locations between trees and they are assumed to represent the majority of the hillslope subsurface.

The live moss layer formed a blanket of relatively uniform thickness across the hillslope, with thicknesses from the upper and lower transects displaying no significant difference (5.6 ± 1.6 cm at the upper, 4.9 ± 1.2 cm at the lower). Microtopography measurements showed high topographic roughness and variation in local elevation (Figure 8). Moss thickness and microtopography may influence hillslope hydrology, as topographic roughness provides places for water to drain or pond, which may promote lateral flow through the permeable mosses.

Soil Characteristics

The soils at the Horseshoe Creek site are developed on till, which contains a range of grains sizes from clays to boulders. Some significant layers of loose rocks were observed at the surface and below the O-horizon. Most of these rocks were somewhat flat and oriented parallel to the soil horizons (with the shortest axis of the rock perpendicular to the soil horizons). Examples of these rock are shown in the bottom-right panel of Figure 4 and in Figure 9. The total soil thickness averaged 58 cm across all the soil pits, measured from the base of the live moss layer to the top of the C-horizon.

Soil horizons were similar between the upslope and downslope sites, with the primary difference being that two downslope sites lacked an Ae horizon, resulting in the average downslope Ae being only 3 cm compared to the average upslope Ae thickness of 8.3 cm (Figure 10). The Ae horizon in downslope pit D-1 was measured at 9 cm, which is comparable to the measured Ae horizons upslope. No other horizon had a significant difference in thickness between the upslope and downslope pits. The soil O-horizons (including dead moss and humus) were on average 12.3±2.5 cm thick upslope and 14.7±2.3 cm downslope; the B1 horizons averaged 9.3±1.2 cm and 10.0±1.7 cm; the B2 horizons averaged 9.3±3.2 cm and 11±3.2 cm; the B3 horizons averaged 6.7±1.2 cm and 9.7±3.1 cm; and the C horizons averaged 9.0±1.0 cm and 12.0±4.3 cm. The O-horizons also include 5.1±1.3 cm of live moss which was not included in the soil layer measurements.

Soil porosity for all layers at all sites was measured at 65-85%, with standard deviations of 5-10% resulting in no significant difference in soil porosity among different soil layers or between the upslope and downslope locations (Table 2).

Soil water content was measured in samples obtained between August 13 and August 18, 2019, when the water table was near its annual minimum, which occurred on August 29 (Figure 5). There were no significant differences in water content between the upslope and downslope sites except in the B2 layer, which has a higher water content upslope. The measured soil water content likely represents the distribution of soil moisture near the annual minimum, illustrating the effects of cumulative evapotranspiration over the summer months.

Rooting Depths and Densities

Roots were measured in each of the soil horizons. To evaluate completeness of the root data, I plotted the root diameter versus cumulative length (Figure 11), which exhibited a power function relationship. Power function relationships tend to be indicative of root and stream networks. These power functions could be used to estimate the cumulative length of the very fine roots (which we assume we under-sampled due to the difficulty of extracting fine roots from the soil matrix) and the few very thick roots (which we purposely under-sampled due to our selection of soil pit sites far from the bases of trees). The largest roots adjacent to tree trunks were not sampled so that we could dig the soil pits by hand and to avoid permanently damaging the trees.

In all the soil pits, the largest volume of roots was located in the O-horizon (Table 2, Figure 12). In this horizon, shallow roots were found to primarily run horizontally, with smaller rootlets extending upwards into the lower moss layer. The few roots that extended to deep depths were often found growing in and through fractures of rocks present in the soil. Although there are few significant differences in root content between

the upslope and downslope sites, root content appears to take up more of the total soil volume at the upslope sites compared to the downslope sites (Figure 12), with the upslope B layers containing significantly more roots than the downslope B layers. The upslope B layers likely contain more roots than the downslope B layers because the upslope water table is at or below the top of the B1 layer (21 cm depth) for almost the entire record of water year 2018 (WY 2018, defined as October 1, 2017 – September 30, 2018), while the downslope water table remains above the top of the B1 layer (18 cm depth) for about 50% of the ET season and almost 100% of the other seasons (Figure 6). Because shallow groundwater is readily available downslope, the downslope trees can use that water to fulfil ET demand by concentrating their roots in the upper soil layers. These trees also develop some roots in the B1 layer to access groundwater when the water table is in the B1 layer (30% of the ET season), but they likely supplement that with soil water, infiltrating rainwater, and shallow lateral flow. For the remaining 20% of the ET season, when the water table drops below the tree rooting depth, the trees would rely completely on these three shallow water sources. Upslope trees likely rely primarily on these sources, indicated by the higher concentration of roots in the O and Ae horizons and the often-inaccessible water table which is at or below the top of the C horizon (48 cm depth) and the deepest observed tree rooting depth for 70% of the ET season. The upslope trees have more deep roots than the downslope trees so that they have a chance of accessing deep groundwater when infiltration and lateral flow are not available, but even those deep roots could only reach the water table for 30% of the 2018 ET season.

Hydrological Analyses

Although the main ET season is defined in this paper as running from June through September, some ET is active before and after the main season. ET begins to rise in early March when it overlaps with the snowmelt season, it peaks during late June to July, and it falls back to near-zero by late October (Figure 13). This supports the hypothesis that ET drives the GW recession throughout the summer. Predicted storage at the downslope location is only negative from early June through mid-September, and it can be positive during this time frame due to storms, when rainfall is higher than average.

Predicted positive changes in groundwater storage can result in groundwater recharge or snow accumulation, and this model does not differentiate between the two. Predicted groundwater table for the downslope site, based on PPT-ET with constant specific yield (0.44) and drainage (2.4 cm/8 days), generally matches the downslope well data, with the table dropping from early May through September, stabilizing for a month, then rising from October through April (Figure 14). A comparison of actual and predicted groundwater level from May 1 through September 29 is shown in Figure 15 (predicted = 1.03*actual, $R^2 = 0.77$).

The predicted downslope groundwater table elevation is above the soil surface from December through the end of the model in early May, which implies snow storage during parts of this time interval. As this model does not incorporate any surface runoff or seasonal variations in drainage, it does not account for large snowmelt events which typically occur beginning in March and continue until the snow has completely melted.

As groundwater table elevations on the hillslope are generally shallow but vary over time, a chart showing how often given soil depths are saturated is more

representative of the water table than a simple average. The observed downslope groundwater table is generally shallower than the upslope groundwater table, but they follow similar patterns for most of the year. At each site, winter and snowmelt seasons overlap greatly (Figure 6). They also show no preferred depth, which would be evident in the groundwater depth exceedance probability distributions as a horizontal line segment, indicating that the top of the groundwater table occupies that elevation for a significant percentage of the season. The fall season shows a preferred depth at both sites (0.25 m upslope, 0.05 m downslope) where the top of the water table is located for the majority (about 60%) of the season. The minimum groundwater table elevation is deepest during the ET season. At the upslope site, there is a maximum depth (0.68 m) that the groundwater table occupies for 50% of the season and does not fall below, but the downslope site's water table does not appear to reach a fixed maximum depth, and it remains above 0.45 m for the entirety of the season.

Discussion

The measured range of *Picea* rooting depths at the Newfoundland field site, where the highest root density was at <10 cm depth and the majority of the root mass (>99.9%) was found within 30 cm of the surface, is similar to prior research findings (Jackson et al. 1996) that boreal forests generally have shallow rooting profiles with 80-90% of roots located within 30 cm of the surface. The findings of my study and Jackson et al. (1996) are somewhat different from recent research which indicates a mean *Picea* rooting depth of 74 cm with a standard deviation of 47 cm (Fan et al. 2017). These differences indicate that species is not the sole determinant of tree rooting depth, and that

there is some variability due to environmental conditions, resulting in *Picea* trees at Horseshoe Creek developing very shallow root systems.

In the same study, Fan et al. (2017) found a relatively strong ($R^2 = 0.7$) 1:1 relationship between tree rooting depth and water table depth across different tree species and biomes, which further emphasizes the strength of the local environment's influence on tree rooting depth. The Newfoundland study site's average tree rooting depth may be equal to the water table depth, as expected, at certain times of the year, but the water table elevation varies by about 40 cm over the course of the ET season (Figure 6) so it is misleading in this case to state that the tree rooting depth is equal to the water table depth.

The water balance calculation, which incorporates precipitation, ET, drainage, and soil specific yield, is a good predictor of groundwater level throughout the ET season (Figure 15). This implies that ET, as the only seasonally variable factor, is the driving force causing the summer groundwater minimum. Prior studies indicate that ET can be the primary factor driving groundwater behavior during summer months in other locations (Gribovszki et al. 2010; Mutzner et al. 2015), further supporting this finding.

Root content is not significantly correlated with water content (Figure 12). Any relationship is primarily influenced by the two labeled data points with the highest and lowest water content in Figure 16. In other studies, low soil water content has been shown to induce stomatal closure and limit tree ET (Reich et al. 2018), so trees may concentrate their roots in wetter soil layers to maximize ET and avoid the drier conditions that force them to close their stomata.

The Newfoundland trees might maintain shallow roots because there is usually sufficient precipitation to meet ET demands by intercepting infiltration near the surface.

There is only a short period of time during the summer months when ET demand is greater than precipitation, and during this time interval trees can supplement infiltrating precipitation with water stored in the moss or organic layers, accessible via their upward-growing rootlets. Warming may increase the duration of this "dry" period (where ET > PPT) or limit moss growth, both of which would limit ET. Therefore, even as the climate warms and the growing season lengthens, ET may remain relatively constant due to the limited water available. Alternatively, trees may grow deeper roots to access deeper groundwater, but this would be a significant departure in current root architecture. This could put the native *Picea* at a competitive disadvantage with invading trees more adapted to warmer climates, as the *Picea* dedicate more energy to accessing water and less to out-growing and out-shading competition. Thus, climate warming could result in large-scale change in tree species diversity, and in the disappearance of the *Picea* boreal forests.

Conclusions

1. As hypothesized, black spruce trees at this site have very shallow rooting depths, with virtually all roots (>99.9%) found within 30 cm of the ground surface. Rooting depths varied slightly with hillslope position, with upslope trees having more roots and a greater proportion of roots extending below the O horizon. These shallow rooting depths suggest that the trees rely on two sources of water for transpiration: a) interception of infiltrating water that is temporarily stored in the live moss and organic horizons, and b) shallow groundwater that declines seasonally.

2. The groundwater table position was described using seasonally separated exceedance probability distributions. During the summer months when ET is highest, the

downslope groundwater table is within 30 cm of the surface for 85% of the season, indicating that trees could draw water from groundwater or from shallow lateral flow. The upslope groundwater table is only within 30 cm of the surface for 5% of the ET season, so those trees likely rely on infiltrating rainwater and shallow lateral flow as water sources.

3. The seasonal variation in groundwater level was modeled with a simple water balance model where changes in groundwater storage were driven by PPT-ET, and the change in storage term was converted to a groundwater depth term by fitting estimated values of specific yield (0.44), and drainage (3 mm/day). The predicted water table depth matched observed depths (Figure 15, $R^2 = 0.77$). Although soil hydraulic characteristics change significantly with depth, the simple model that uses properties of the moss and organic horizons for specific yield and observed drainage rates fits the data well. This suggests that the properties of the shallow soil and moss horizons regulate much of the current relationship between ET demand and water table depth. This may change in the future if ET demand significantly lowers the water table below the moss and organic horizons.

4. The agreement between the model and observed data also implies that ET and lateral flow are major influences on the groundwater table during the ET season, supporting most of the second hypothesis. I predicted that trees would take up groundwater directly, but based on their shallow root systems and the greater depth to groundwater at the upslope site, it is more likely that ET forces the groundwater table decline by intercepting infiltrating water before it can recharge groundwater storage rather than directly removing water from groundwater storage. Because this mechanism

relies on precipitation and transient soil water, this source of water will be exhausted by an extension of the growing season with global warming. It may especially impact the downslope site, as upslope trees intercept a greater proportion of shallow lateral flow before it can reach the downslope trees. The downslope trees currently have shallower roots and it will be more difficult for them to adapt to deeper water tables.

5. Root content and soil water content were weakly correlated, with greater water content generally being associated with greater root content. Soil bulk density and porosity did not significantly change among different soil layers, so these soil factors cannot show any relationship with the root and water content. The water and root contents may exhibit only a weak correlation because water contents were measured in August, at the annual groundwater minimum and after trees have been taking up water for ET for months. Further research could measure soil water content over time, especially at the beginning and middle of the ET season, in order to better determine relationships between root content and soil water content.

Table 1. Characteristics of Newfoundland study site.

	Horseshoe Creek Watershed, Newfoundland, Canada
Hydrologic Location	Hillslope
Elevation (m)	300
Dominant Tree Species	Black spruce
Soil Description	Leached podzol, recently glaciated
O-horizon Thickness (cm)	21 ± 6
Tree Density (m^2/m^2)	0.0079 ± 0.0007
Mean Annual Temperature (°C)	3.6
Mean Annual Precipitation (mm)	1095
Mean Annual ET Demand (mm)	475 (43% of MAP)

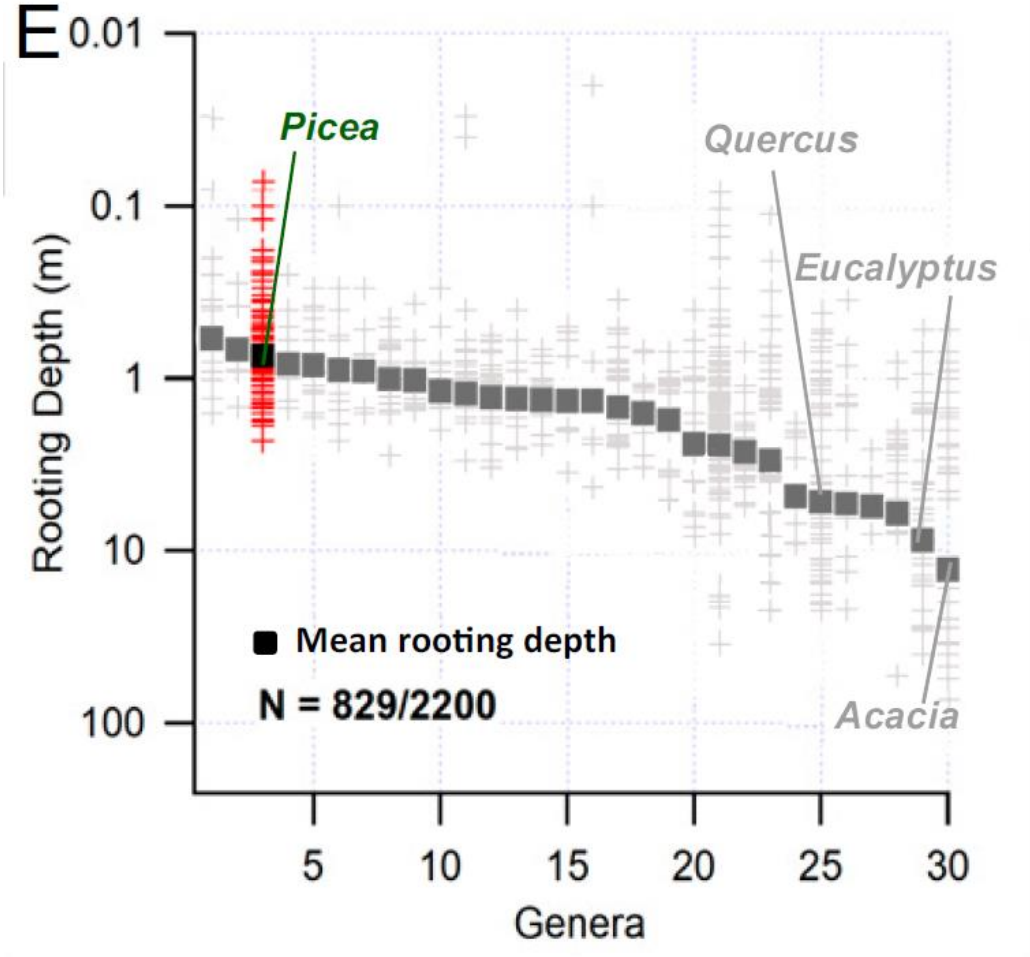

Figure 3. Tree rooting depths by genus. From Fan et al. (2017), with colors changed to highlight the genus *Picea*, which is the dominant genus at the study site.

Figure 4. Photos of soil pits and roots in Newfoundland. Top left, the soil surface after removing the live moss layer. Top right, collaborator Zachary Gates standing in an in-process pit (photo by Susan Ziegler). Bottom left, the face of pit U-1 with soil horizons and roots visible. Bottom right, fine roots attached to a rock with a standard-size Sharpie for scale.

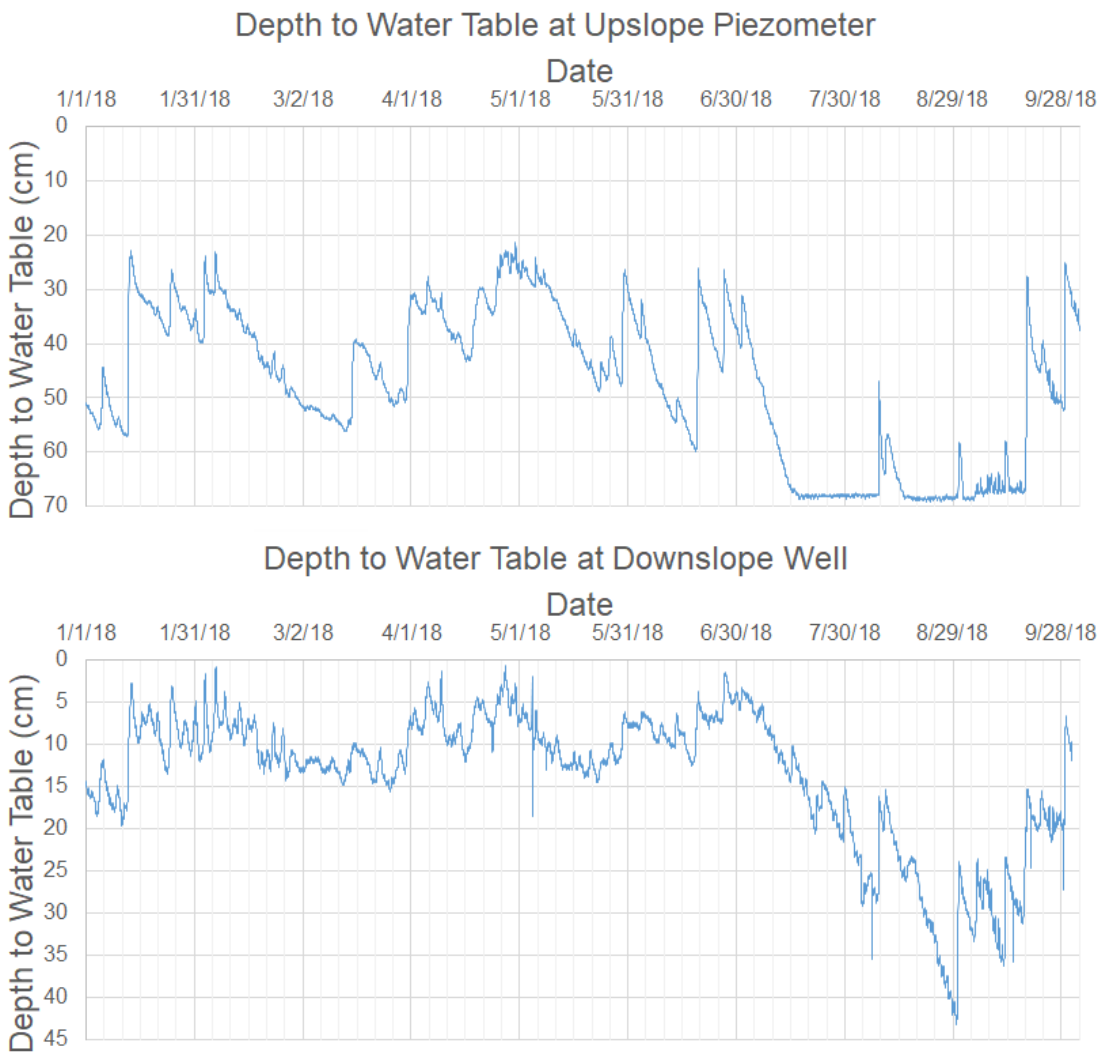

Figure 5. The depth to the water table at the upslope piezometer and downslope well for January 1, 2018 through September 30, 2018. Note the overall decline in water table elevation throughout the warmer months (May through August), and the annual minimum in late August.

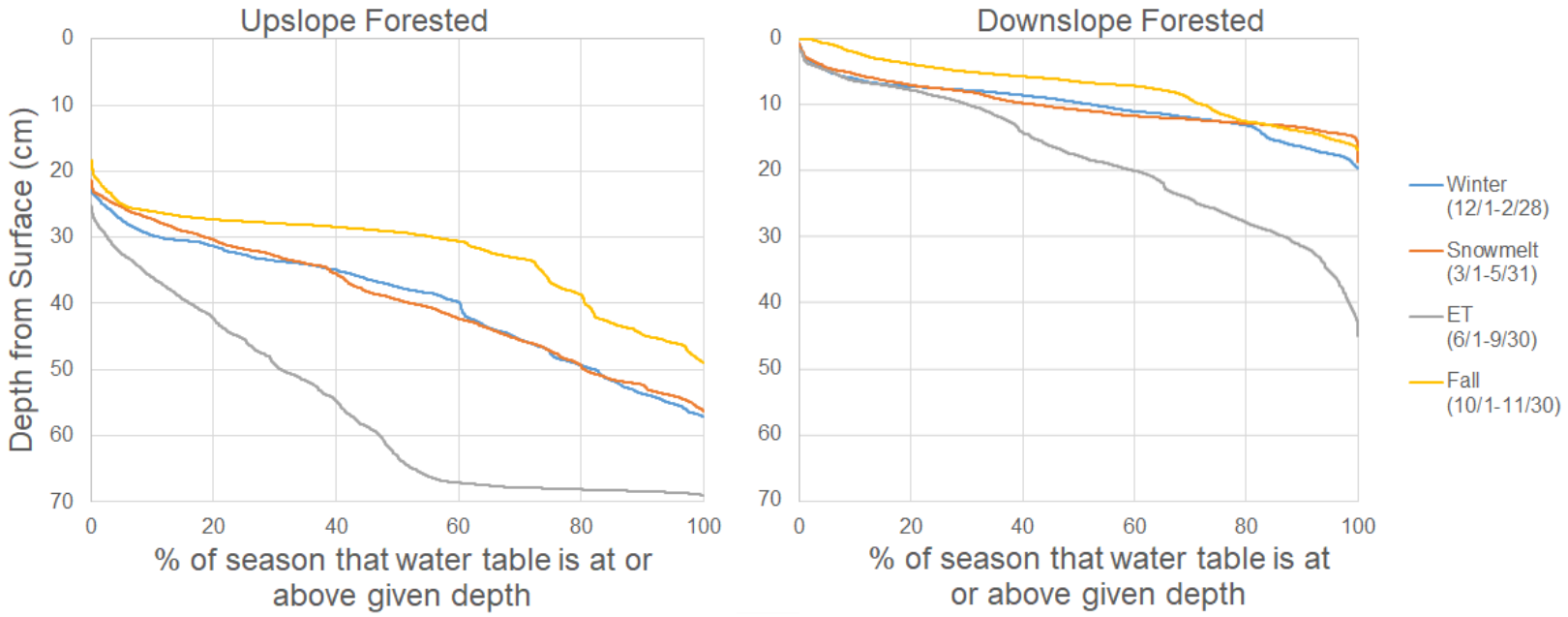

Figure 6. Groundwater depth distributions for WY 2018 for upslope and downslope locations at the study site. The depth distributions are by season, with seasons generally determined by the presence of snow ("winter", 12/1-2/28), warming air temperatures with snow present but melting ("snowmelt", 3/1-5/31), warm air temperatures with no snow present ("ET", 6/1-9/30), and falling air temperatures with no snow present ("Fall", 10/1-11/30).

Table 2. Data collected from soil pits in Horseshoe Creek Watershed, Newfoundland, Canada. Some measurements were made for each layer in each soil pit (layer thickness, root content, water content, porosity), and some measurements were made once per pit (moss layer thickness*, tree density). Note that pits D-2 and D-3 had no Ae layer.

*Moss thicknesses reported here are the measurements made once at each pit; more moss thickness measurements were made along transects and are not reported in this table.

Soil Pit, Layer	**Layer Thickness (cm)**	**Root Content (% total vol.)**	**Water Content (% total vol.)**	**Porosity (% total vol.)**	**Live Moss Thickness (cm)**	**Tree Density (m^2/m^2)**
U-1					4	0.404
O	15	2.0	20.0	-		
Ae	7	4.6	23.0	66.3		
B1	10	2.6	36.1	79.7		
B2	13	0	34.1	82.6		
B3	8	0	28.4	64.4		
C	9	0	23.9	68.2		
U-2					4	0.420
O	12	5.2	20.0	-		
Ae	8	2.0	27.6	84.7		
B1	8	2.9	34.3	84.4		
B2	7	0	40.0	88.9		
B3	6	0	26.2	87.6		
C	10	0	24.2	87.7		
U-3					6	0.441
O	10	11.4	20.0	-		
Ae	10	2.9	36.8	78.3		
B1	10	5.0	57.3	82.4		
B2	8	0.1	42.0	83.8		
B3	6	0.1	27.2	82.4		
C	8	0	28.1	82.3		
D-1					5	0.347
O	16	0.9	21.0	-		
Ae	9	1.6	36.2	66.6		
B1	11	0.6	32.3	71.3		
B2	10	0	31.1	72.1		
B3	8	0	29.9	83.5		
C	8	0	25.4	68.5		
D-2					4	0.356
O	16	4.8	21.0	-		
B1	11	1.0	30.9	75.5		
B2	9	0	21.8	62.9		
B3	10	0	24.0	66.3		
C	9	0	24.8	68.7		
D-3					4.5	0.403
O	12	22.0	21.0	-		
B1	8	0	25.2	75.8		
B2	15	0	24.9	81.5		
B3	14	0	21.2	73.1		
C	16	0	18.3	91.4		

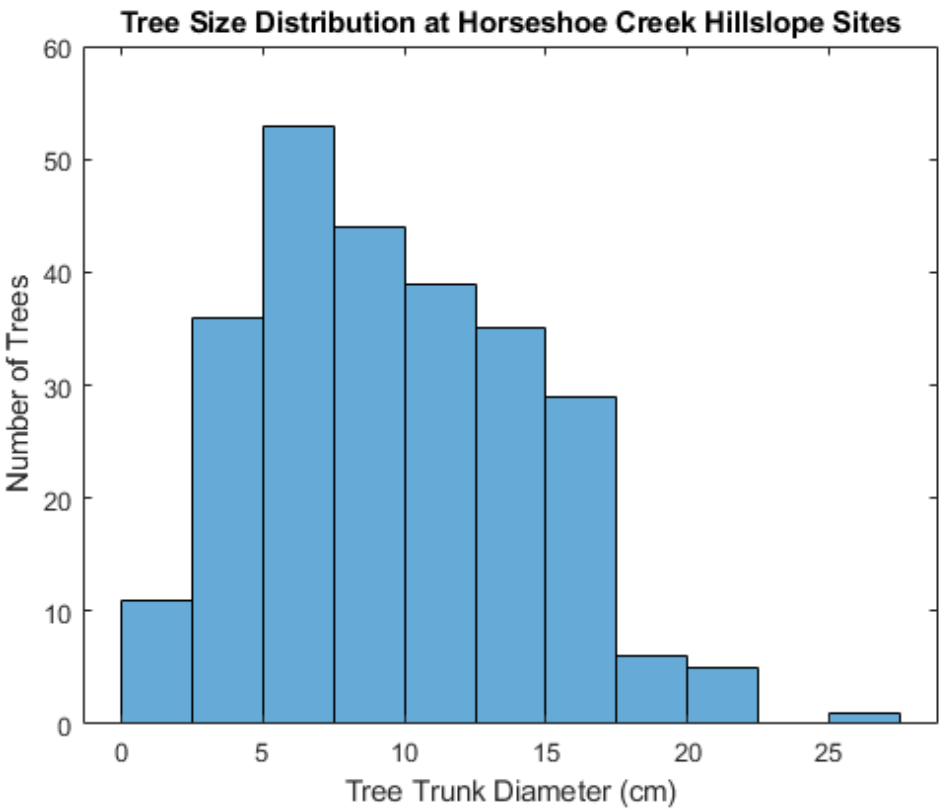

Figure 7. Tree size distribution. The majority of trees (91%) have a trunk between 2.5 and 17.5 cm in diameter.

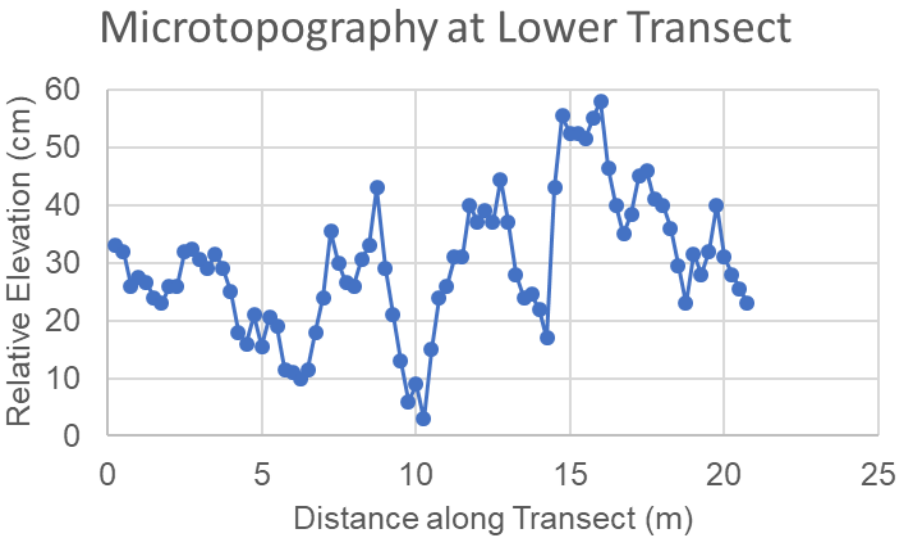

Figure 8. Relative elevation measured along the lower hillslope transect. Some high points, such as the one at 8.75 m along the transect and 43 cm relative elevation, are due to fallen tree trunks that crossed the transect.

Figure 9. Examples of rocks found in the soil pits. Left, a flat rock from pit D-1 positioned to match its in-pit orientation on top of a standard 5-gallon bucket. Right, the face of pit D-1 with some protruding rocks and some holes where rocks were removed, and a meterstick for scale.

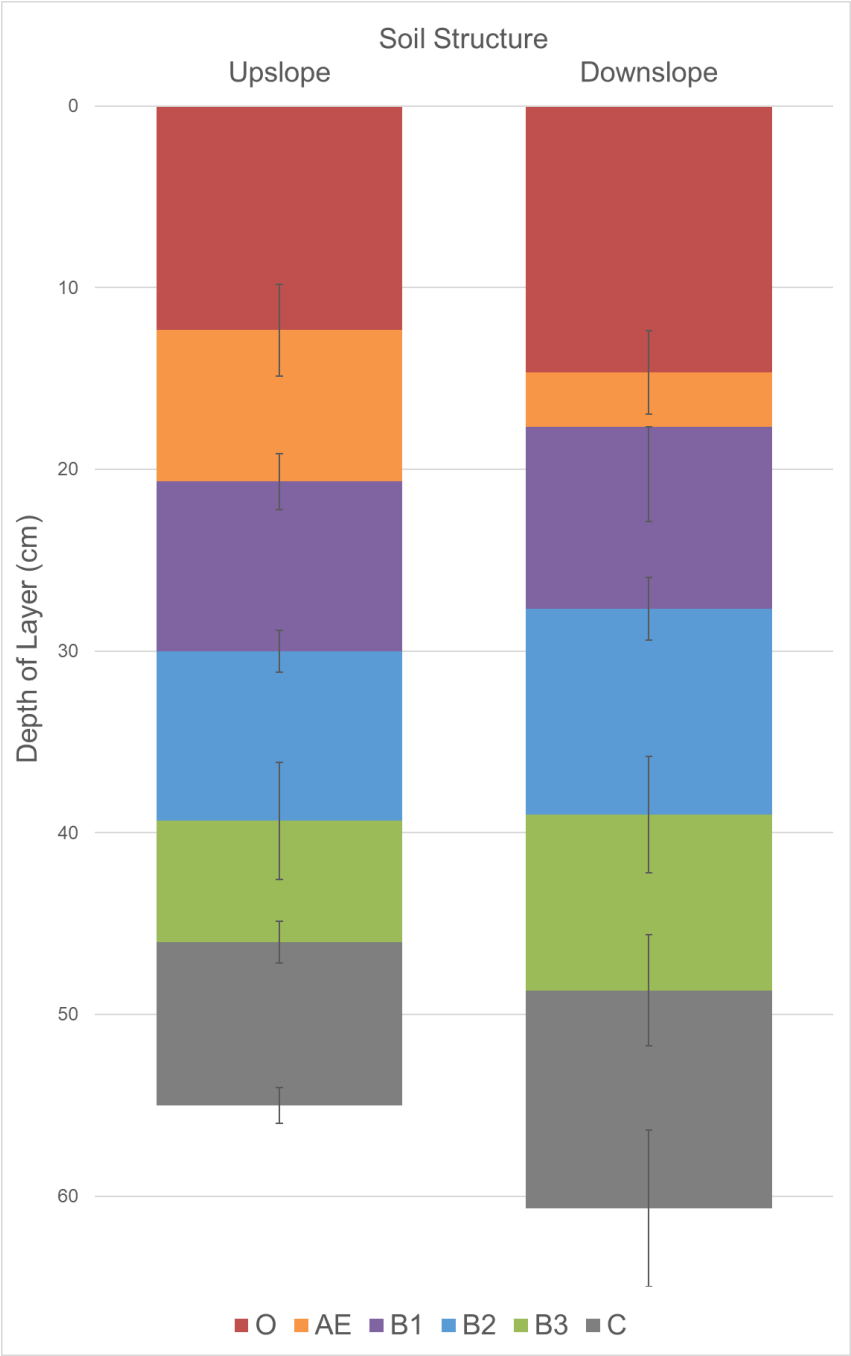

Figure 10. Average soil structure compiled using the average thickness of soil horizons obtained from 3 soil pits each in the upslope and downslope transects. Error bars indicate one standard deviation. The upper error bar for the downslope Ae layer overlapped completely with the error bars for the downslope O layer, so that layer's upper error bar was omitted.

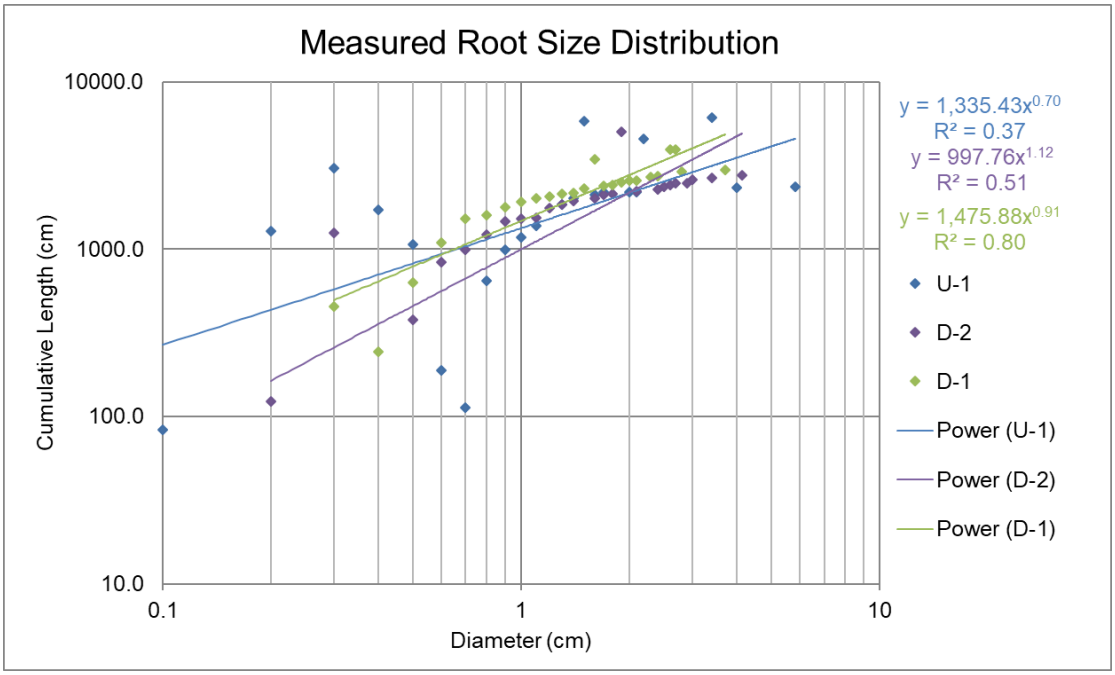

Figure 11. Root diameter vs cumulative length graphs for the upslope soil pit U-1 and downslope soil pits D-2 and D-1 in Newfoundland. The lines of best fit are length = a(diameter)^b and have R^2 values ranging from 0.37 to 0.80. The coefficients range from 997.76 to 1475.88, and the exponents range from 0.70 to 1.12.

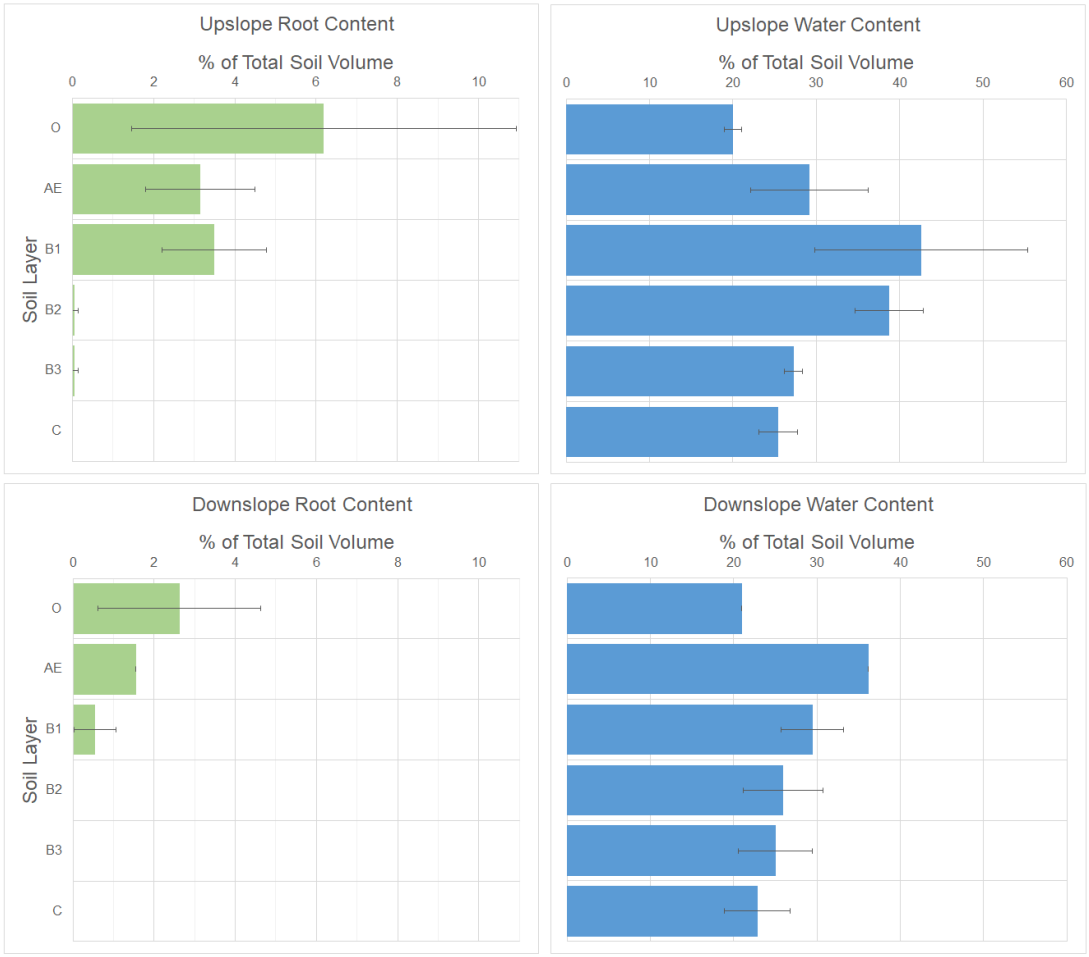

Figure 12. Volume percentages of water content and root content by soil horizon. Root and water volume data were obtained from soil pits along the upslope and downslope transects, from August 13 to August 18, 2019. Root and water content are expressed as a percent of total volume for each soil horizon. Error bars represent one standard deviation; note that for the downslope locations, only one pit had a distinct Ae layer and therefore only that sample was counted (giving SD = 0 for the Ae layer).

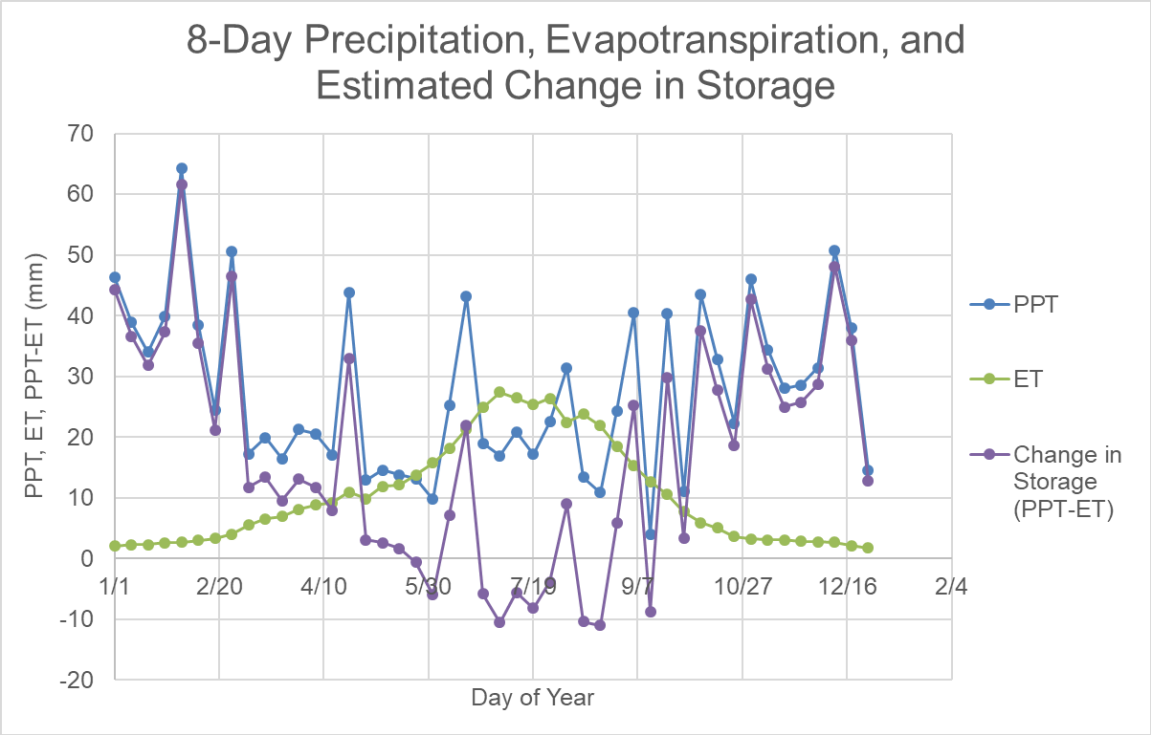

Figure 13. Precipitation, evapotranspiration, and estimated change in storage (as PPT-ET) for Horseshoe Creek watershed. Each variable is the 8-day sum, averaged over multiple years (5 years for ET, 4 years for PPT). Precipitation is variable throughout the year with no notable seasonality, and ET peaks around the start of summer (late June through July). Water is removed from storage from early June through mid-September due to ET demand. Storms can drive intervals of positive storage during this period of high ET demand.

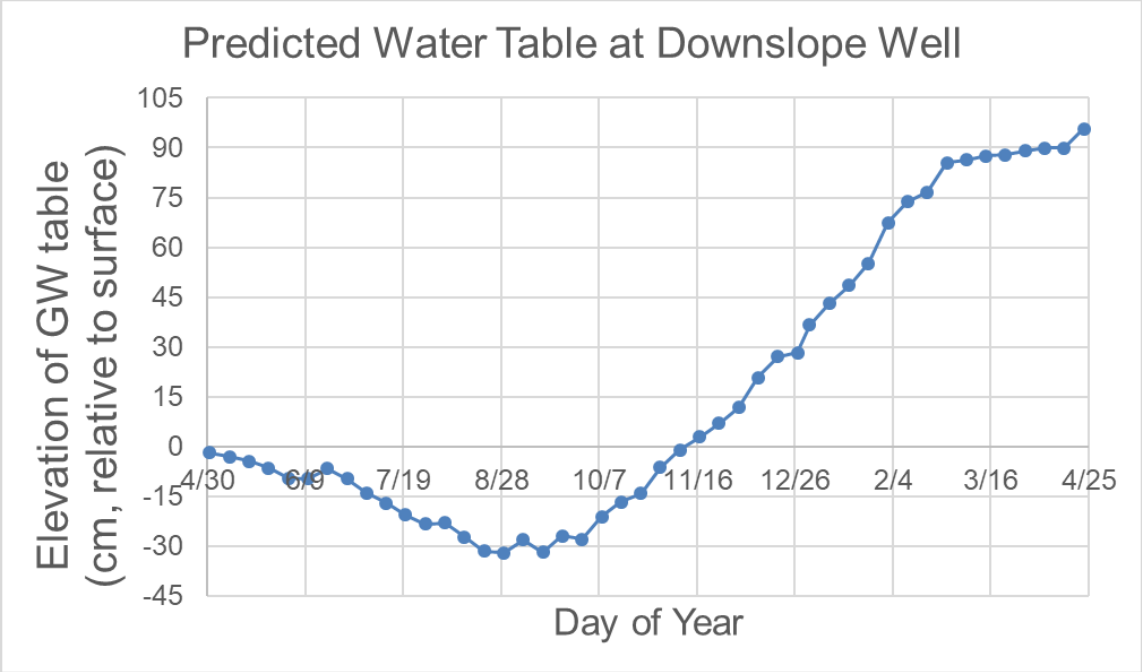

Figure 14. Predicted water table based on PPT-ET, specific yield of the soil (0.44), and constant daily drainage (2.25 mm/day). Where the water table is above 0, the model predicts storage as either snow or groundwater recharge. May 1 was chosen as the start date for the model because the actual groundwater table was near 0 at that date.

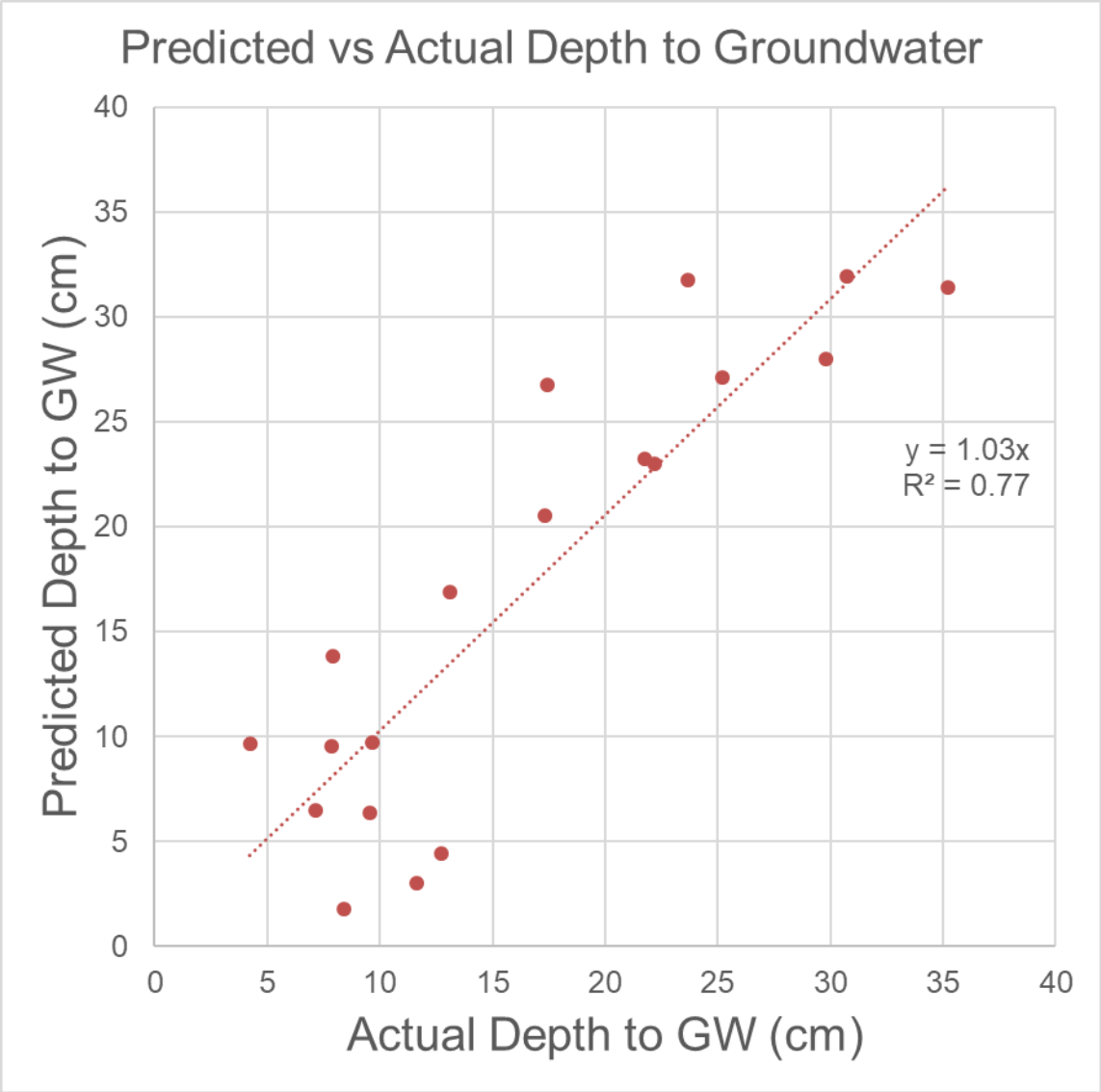

Figure 15. A comparison of actual and predicted depth to groundwater table for May 1 through September 29. Both are 8-day averages, with actual depth to groundwater data from 2018 and predicted groundwater data from the model described above.

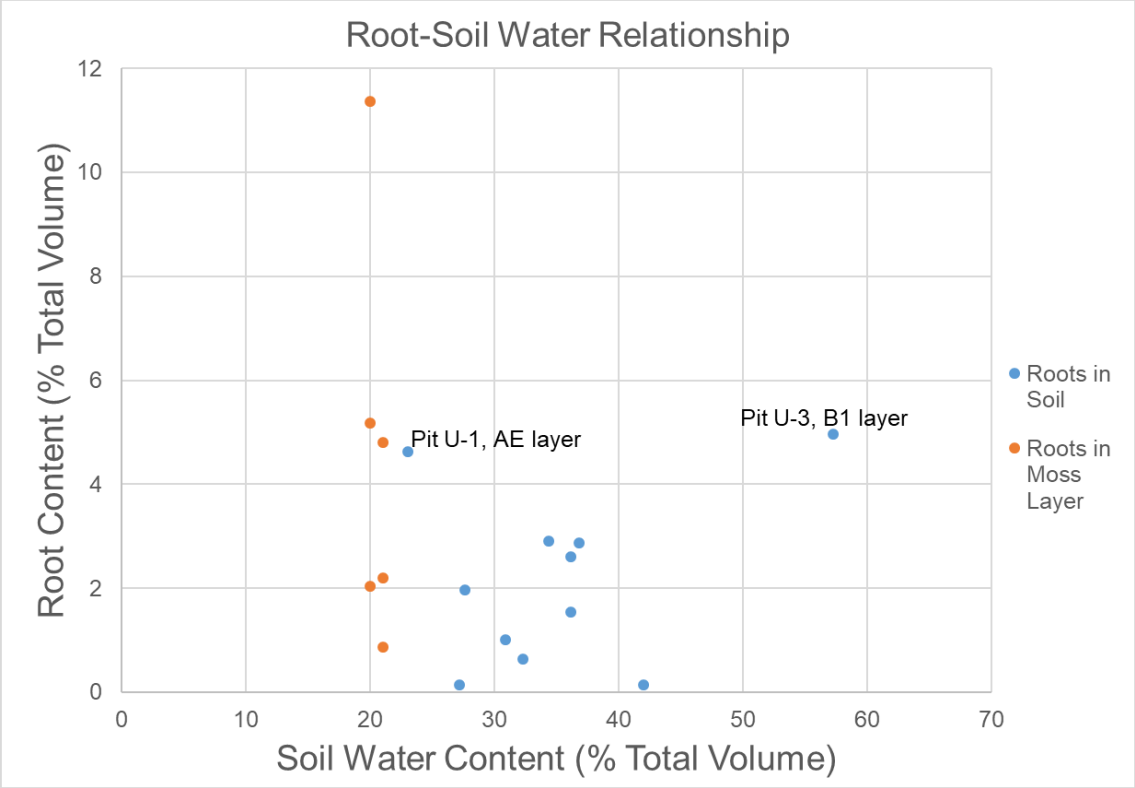

Figure 16. The relationship between root content and soil water content for the measured soil layers at all pits, excluding layers where root content was 0. Data is separated by roots growing in soil and roots growing in the moss layer. Any relationship between root content and soil water content for soil roots is strongly influenced by the two points labeled on the graph above.

Chapter 3: Seasonal and Diurnal Influence of Evapotranspiration on Catchment Streamflow and Water Specific Conductance

Introduction

In the previous chapter, I examined the relationship between ET and water table depth on the hillslope. In the Newfoundland wet boreal climate, ET demand does not exceed precipitation during most of the growing season, and groundwater levels can be predicted by a simple model incorporating PPT-ET, specific yield, and drainage. Groundwater and shallow throughflow during storms also contribute to streamflow. Thus, seasonal variations in ET will also affect streamflow. In many catchments, however, the ET effects on streamflow can be muted by downslope movement of water that replaces water lost to ET. Water supplied from lakes or wetlands can also replace water lost from the catchment as ET, which can also mute the ET signal in the stream. Riparian ET losses adjacent to the stream, however, can increase overall catchment losses to ET. These near-stream losses or gains can often be observed as diurnal variations in streamflow discharge. Many previous studies of catchment water balances, ET and streamflow focus on using streamflow to estimate catchment ET (PPT-Runoff). Other studies focus on using diurnal groundwater or streamflow variations to evaluate local diurnal influences of ET while acknowledging the need to extend this research to seasonal timescales (Bond et al. 2002; Gribovszki et al. 2008, 2010; Mutzner et al. 2015).

The previous chapter of this work indicates that ET is a major component of the water balance for the Horseshoe Creek catchment, and it has a significant seasonal impact on groundwater level. ET likely influences streamflow by limiting hillslope soil and groundwater contributions to streamflow, which decreases stream discharge.

Limitations on hillslope contributions to streamflow would likely also limit nutrient and carbon export. Water is a primary mode of transportation for solutes such as DOC to exit catchments, and DOC fluxes to aquatic systems prevent soil organic carbon from entering longer-term mineral carbon storage (Ziegler et al. 2017; Bowering et al. 2020; Knapp et al. 2020). In addition to limiting nutrient and carbon export, these minima also act as feedback to limit ET itself, thereby influencing carbon cycling from multiple ends (Reich et al. 2018).

Many catchments in boreal landscapes contain lakes and wetlands. These features contribute to short and long term water storage. They can supply water to downstream rivers, offsetting losses due to ET from other parts of the catchment. Lake contribution to streamflow can constitute a significant proportion of total stream discharge; prior research in a small (1.1 km^2) boreal forest catchment indicated that a headwater lake was the primary source of stream discharge outside of periods influenced by precipitation (Leach et al. 2017). Long residence times in lakes can attenuate and delay stream discharge peaks in response to precipitation events (Arp et al. 2006; Leach et al. 2017). Long residence times also allow direct surface evaporation and ET to concentrate solutes and isotopes in lakes, giving outflow a distinct, high-conductivity signature (Wetzel 2001; Leach et al. 2017).

Therefore, data on lake outflow and associated conductivity in comparison with downstream streamflow and conductivity can provide information on the relative contributions of lake water and hillslope contributions to streamflow, and the effects of ET on these contributions. If lake outflow is the primary contributor to stream discharge, stream discharge will resemble the conductivity of the lake. The conductivity of both

would be expected to increase over the summer months as evaporation concentrates the solutes present in the lake water source (Wetzel 2001). Evapotranspirative concentration of infiltrating water can also occur in forested landscapes. Therefore, groundwater, shallow lateral flow, and lake water can all increase in conductivity as they pick up dissolved ions from soil and bedrock and they become concentrated due to evaporation. Long residence times in lakes and groundwater allow time for more ions to enter the water (Gurnell and Fenn 1985; Wetzel 2001; Graly et al. 2017). Forest vegetation adds root exudates to soil and contributes to mobile organic carbon stocks (Brantley et al. 2017), providing ions that would allow shallow lateral flow to increase somewhat in conductivity even over short residence times. Fluctuations in conductivity have been observed over diurnal and seasonal timescales in glacial outlet streams, and have been attributed to mixing of water sources with different conductivity and to the addition of high-conductivity water during times of high streamflow (Gurnell and Fenn 1985; Graly et al. 2017).

Diurnal fluctuations of stream discharge and shallow groundwater level have been observed in various ecosystems, and they can be caused by factors such as the timing of daily snowmelt and freeze-thaw processes and water drawdown due to evapotranspiration (Gribovszki et al. 2010; Mutzner et al. 2015). The pattern of water level changes varies depending on the mechanism causing the diurnal cycle, with evapotranspiration generally creating an early morning maximum and afternoon minimum in groundwater level and streamflow, with potential for streamflow to lag behind groundwater level (Gribovszki et al. 2008). Other mechanisms such as melting can occur at the same time, but with an

opposite direction and a signature distinct enough to distinguish between the two processes (Mutzner et al. 2015).

The relationship between solute concentrations and stream discharge can indicate the pathway that the water takes through the catchment: increasing concentration with increasing discharge is an example of "mobilization behavior", which can be caused by throughflow flushing solutes from the soil, while decreasing concentration with increasing discharge is "dilution behavior" and is often associated with source limitations of the solute (Knapp et al. 2020). The timing and magnitude of peaks in concentration and discharge, and any changes in the timing and magnitude of these peaks, could also indicate the source of streamwater; a direct connection between ET and the stream gauge causes a discharge peak in the early morning, around 7 am, corresponding to the onset of ET (Gribovszki et al. 2010). A gauge height or discharge peak at a different time would give a measurement of how long it takes the source water to reach the stream gauge.

Research Questions

1. When is the annual streamflow minimum? Does it occur simultaneously throughout the watershed? Does it occur simultaneously with the groundwater minima?
2. Is the seasonal increase in stream baseflow conductance consistent with evaporative concentration of water that contributes to streamflow? Are there significant differences between upstream and downstream conductivity that help us understand forest evapotranspiration?

3. What do the diurnal variations in streamflow and conductivity indicate about the source of contributions to streamflow in summer months? Do changes in timing and magnitude of variations indicate different sources?

Site Description and Methods

Study Site Characteristics

Horseshoe Creek Catchment can be divided into two regions that are morphologically different but have similar basin areas. The upper catchment contains lakes and wetlands, discontinuously connected by low gradient streams. The lower catchment has a low-gradient upper region, but it is primarily characterized by steep hillslopes that contribute to a steep, boulder bed channel (Figure 17). Water level indicators and conductivity sensors were installed by the Memorial University research team at two gauge locations in the watershed in 2014 to monitor streamflow from the upper basin and lower basins. The distance between these two gauge locations is 5.25 km measured along the stream channel. The outlet of the largest lake in the upper catchment discharges into Horseshoe Creek just above the upper stream gauge. Therefore, stream discharge and conductivity at the upper gauge are influenced by wetland and lake processes. The lower stream gauge monitors the combined streamflow and water chemistry that result from the upper basin, including the lake contributions, but also the hillslope contributions from the boreal forest in the lower watershed. These hillslopes have gradients of 8-10% that contribute directly to the stream without an

intervening floodplain. There is a riparian wetland region in the upper part of the lower basin which separates the steep hillslope region from the stream (Figure 17b).

Figure 18 shows photos of the lake outlet, the upper gauge, and the lower gauge. These differences in lake influence, topography, and riparian zones could influence the timing, magnitude, and conductivity of waters that contribute to streamflow. For example, the steeper Lower Horseshoe drains more effectively, leading to deeper groundwater tables during summer months and perched shallow lateral flow in the organic horizon during snowmelt and other wet seasons (Bowering et al. 2020). Evapotranspiration on hillslopes would likely lead to step-wise water table declines. Forest evapotranspiration and drainage would lead to a deeper GW table in Lower Horseshoe during summer months, as shown in the previous chapter. Therefore, Upper Horseshoe basin and the upper wetland areas of Lower Horseshoe are likely the only areas with a stream-adjacent groundwater table shallow enough to generate a sinusoidal ET-driven stream response. This assumes that there is not an effective riparian zone along the steeply incised river reaches between the upstream and downstream gauges.

Electrical conductivity values range from near zero (0.5- 1.5 μS/cm) in precipitation to over 70 μS/cm in some lake and GW measurements, with shallow lateral flow acting as a source of both discharge and conductivity in the stream system (Table 3). Therefore, stream conductivity will be linked to stream depth at the Upper Horseshoe gauge, and the Lower Horseshoe gauge will experience the same pattern with the addition of a lag time to account for the water flowing downstream.

Gauge Height and Conductivity Data

The Horseshoe Creek stream gauges were installed at two locations by a research team lead by Dr. Susan Ziegler of Memorial University of Newfoundland. The two sites were selected because they divide the watershed into two roughly equal parts and they are accessible by road. Water depth, conductivity, and temperature data were recorded at each gauge every half hour. The Canadian Forest Service in Corner Brook, NL assisted in gauge maintenance and discharge measurements.

Rating Curves, Velocity, and Determination of Discharge

To estimate discharge from continuous records of gauge height, I used GH-discharge rating curves constructed by Dilanka Athukorala (Athukorala 2020). These rating curves were developed using velocity and area measurements for low to moderate flows, and estimated velocity and area measurements for high flows. High flows during snowmelt or storm events were difficult to gauge, therefore flow resistance equations were used to estimate velocity and calculate discharge for these higher flows. Flow resistance equations require data on stream gradient, grain size, and channel cross sectional area. To evaluate the resulting relationships, particularly the gauge height-velocity relationships, I compared the Horseshoe Brook data with velocity, discharge, and flow resistance data obtained from USGS measurements of similar steep, boulder bed, small streams in the boreal forest region of Northern Maine. Gauge height-velocity relationships that were developed were used to evaluate travel times in the analysis of diurnal patterns.

Seasonal Evaporative Concentration and Effects on Streamflow

The electrical conductivity of the streamwater, groundwater wells, and lysimeters was observed to increase over the course of the summer. These changes could result from either evaporative concentration of water or changes in water sources. To evaluate the evapotranspiration component of this increase in electrical conductivity, I used the ET calculations described in the previous chapter and compared the cumulative ET amount to the electrical conductivity of stream baseflow.

The two stream gauges receive water from different sources. The upstream site is downstream of a significant lake, therefore, lake turnover and mixing significantly effects electrical conductivity. Thermal turnover mixes the lake in the spring and fall. Spring turnover likely mixes solute-rich deep waters with fresh snowmelt. Thermal stratification of the lake in the summer will generate surface waters that become warmer and more solute rich over the summer months (Wetzel 2001). This is the water that leaves the upper lake and contributes to the upper Horseshoe gauge. Therefore, comparison of the conductivity versus time and discharge relationships of the two gauges can be used to evaluate both lake processes and evapotranspiration that occurs on the hillslope over the summer months.

Hydrograph Separation Analyses

Chemical hydrograph separation analyses use the characteristics of end-member samples to determine the contributions of these sources to streamflow (von Freyberg et al. 2018). In this analysis, stream contributions were assumed to come from 2 end-members with distinct conductivity values. The first end-member is precipitation, in the

form of rain or snowmelt that contributes a dilute "new" source to the streamflow. The other source is "old" water, defined as water that is in the system prior to a snowmelt or rainfall event. For the summer months, the "old" water component is the baseflow, the conductivity of which increases systematically over the summer months. The percent of total discharge attributed to old water was calculated as:

$$Q_{old} = (C_{stream} - C_{new}) / (C_{old} - C_{new}) * Q_{stream}$$

where Q represents stream discharge and C represents conductivity. Values of end-members are as follows: C_{new} = 1.5 μS/cm. The old endmember (C_{old}) was calculated by fitting linear equations to the streamflow baseflow conductivity over the course of the ET season. A summary of the conductivity of different water sources in the catchment is listed in Table 3.

Evaluation of Diurnal Variations in Gauge Height and Conductivity

The stream gauge height and conductivity time series data showed well-defined diurnal patterns for various portions of the year. Therefore, I analyzed the time series data to determine the timing of maximum gauge height and conductivity at the two gauge locations to provide information on the mechanisms and potential sources of the diurnal pattern (Gribovszki et al. 2010). I developed a Matlab code to find the time of day at which the maximum depth and conductivity occurred. I removed days with greater than 1 cm of precipitation in order to separate hydrograph events from diurnal patterns, and ran the code on data from each of the two stream gauges for the period from May 1 to August 30 in 2018, resulting in 60 days during this time period with less than 1 cm of precipitation.

Results

Seasonal Variations in Catchment Stream Flow and Conductivity

Streamflow is relatively constant throughout the year at both gauges, with pulses occurring during three main periods: as a result of winter storm/melt events (January-February), snowmelt (April-May), and fall storms that occur during ET slowdown (September-October. In addition to these main pulses of streamflow, streamflow slightly decreases through the summer period when ET is greater than precipitation, e.g. July and August (Figure 19). The summer decrease in streamflow reflects the decrease in groundwater table on the hillslope (Figure 5).

Conductivity similarly undergoes seasonal changes. It decreases in January and the beginning of May as snowmelt dilutes the stream, and it increases throughout the summer as ET concentrates solutes in the lakes and groundwater that feed the stream. The impact of thermal stratification in the lake and concentration of solutes over the course of the summer is magnified by the shallow outflow path, which indicates that lake outflow primarily draws water from the upper layer of the lake (Figure 18). The lake freezes in the winter, and it undergoes thermal mixing and turnover during the spring and fall as the surface water becomes cooler and denser than deeper water. This prevents a permanent concentrated upper layer from forming, limiting its presence to the summer months. Although lake water outflow prior to turnover is likely dilute, the spring turnover and mixing brings high-conductivity water to the surface. The 2018 spring mixing event likely occurs on June 15, when conductivity at the upper gauge suddenly

increases and remains elevated for a week before mixing with new precipitation and shallow groundwater inflow (Figure 20).

The seasonal changes in conductivity are visible in data from both gauging stations, but the lower station shows a greater increase in summer conductivity compared to the upper station; the upper station has greater conductivity for most of the year, but the lower station has greater conductivity during July and August (Figure 19). This implies that the conductivity source for most of the year is the lake, as that is closer to the upper gauge, and the groundwater and runoff that contribute to streamflow at the lower gauge dilute the conductivity during most of the year. Periods where the upper gauge recorded near-zero conductivity (early January, mid-March, and early August) are likely due to partial exposure of the probe during times of decreased streamflow. The stream is deeper at the lower monitoring site, so an exposed probe at the upper site would account for the fact that the conductivity remains above 10 μS/cm at the lower site during the same time periods.

Warm Season Reduction in Streamflow and Concentration of Solutes

Streamflow decreases and conductivity increases over the course of the summer at both the upper and lower Horseshoe Creek stream gauges (Figure 20), including a linear increase in conductivity over the month of May (Figure 21). This pattern is associated declining limb of the snowmelt hydrograph. Snowmelt provides dilute water sources from shallow lateral flow and flow through or at the base of the snowpack.

Throughout May 2018, the Upper Horseshoe gauge recorded higher conductivity and greater diurnal variations compared to the lower gauge, and both recorded increasing

conductivity throughout the month (Figure 21). These factors indicate that snowmelt runoff dilutes the concentration of solutes between the two gauges, as hillslope snowmelt contributions are greater at the lower gauge and snowmelt overall declines throughout May. This also implies that the lake is a primary source of conductivity during the snowmelt period. Streamflow conductivity at the lower gauge was lower, suggesting dilution by hillslope processes over the distance between the two gauges.

Over the summer months, stream baseflow decreases by 65% at both gauges, and electrical conductivity increases approximately three-fold at the upper gauge and six-fold at the lower gauge. These differences between the two gauges suggest that the source of water that contributes to streamflow in Lower Horseshoe is different than in the upper basin. This increase in conductivity in the stream occurs over the ET season, at the same time as the decrease in piezometer and well depth (Figure 5) and the negative hillslope water balance (Figure 13).

In the previous chapter, I calculated the hillslope water balance. I also calculated the cumulative ET for the summer months and compared it to the summer baseflow conductivity for lower Horseshoe Creek. These data indicate a strong linear correlation (Conductivity = 0.2135*(Cumulative ET) + 24.524, $R^2 = 0.9471$) between cumulative ET and baseflow conductivity (Figure 22).

Warm Season Hydrograph Separation

The relationship between cumulative ET and stream electrical conductivity observed at the downstream gauge suggests progressive ET concentration of water contributed from the hillslopes to streamflow accounts for the observed seasonal changes

in streamflow conductivity. This further suggests that water taking direct pathways from precipitation to the stream ("new" water) contributes little to streamflow during the warm season. To evaluate this question, summer season streamflow was separated into "old" and "new" water components using precipitation and baseflow as end-members for electrical conductivity values. Baseflow conductivity were used for the high conductivity end-member. Storm events occurred which diluted streamflow conductivity, but baseflow between storm events increased continuously over the summer months (Figure 23b). Hydrograph separation analysis conducted using these values indicates that the majority of streamwater is old water that has taken longer or evaporative subsurface pathways, rather moved to the stream on direct paths from rainfall to streamflow (Figure 23a). These data suggest that lake outflow is the primary contributor to baseflow at the upper gauge, and that deeper groundwater and/or evaporatively concentrated shallow lateral flow is combined with lake water to comprise baseflow at the lower gauge.

Diurnal Variations in Streamflow and Conductivity

Although ET on the hillslope, in riparian zones, and from the lake results in warm season streamflow reduction and concentration of solutes at both gauges, ET is a diurnal process. Evaporation from the lake takes place only when there is a vapor pressure difference between the air masses over the lake and the lake surface. Transpiration by plants takes place during daylight hours. Therefore, diurnal variations should occur as local water tables are drawn down during the day and recover at night. Vegetation near streams at baseflow can intercept water on its way to the stream during the day and allow it to flow to the stream at night. Variations in the timing of diurnal signals between the

two gauges may identify differences in ET responses at the two locations. Diurnal signals might be absent from source contributions if the dominant process does not generate a recovery signal.

Observations of the two Horseshoe Creek gauges indicate that stream depth and conductivity both undergo diurnal variations at the two stream gauges; example 5-day periods with minimal precipitation interference are shown in Figure 24. The example 5-day periods are different for the upper and lower gauges due to different behaviors at the gauges; there was a small (3-mm) rainfall event on June 3, and the upper gauge recorded an event hydrograph which rose and fell quickly before the diurnal pattern resumed, while the lower gauge displayed a diminished diurnal pattern through June 8. It was difficult to find a 5-day period where the lower gauge was completely free of precipitation influence, as rainfall generally occurred at least twice per week and the lower gauge often displayed a diminished diurnal cycle for 1-5 days after rainfall. The differing behaviors between the two gauges could be due to differing travel times to the two gauges; when rain falls on the lake, it likely flows directly to the upper gauge, which receives little other input, but the lower gauge receives water that travels farther along the hillslope as shallow lateral flow, extending the period of influence that a precipitation event has on that gauge.

Data compilations indicate that the maximum discharge and conductivity generally occur at the same time from May through September, excluding days with greater than 1 cm of rainfall (Figure 25). The discharge and electrical conductivity are both greatest at the upstream site around 5 pm (standard deviation = 2 hours), and at the downstream site at midnight (standard deviation = 1 hour), giving a timing difference of

7 hours. There is no discernable change in timing over the course of the season, though there were more days with significant rainfall or missing data in July and August, which results in fewer data points for those months (Figure 26). Despite the lower gauge being more influenced by precipitation events, the maximum depth was more predictable at that gauge (standard deviation was ± 1 hour at the lower gauge, compared to the upper gauge's standard deviation of ± 2 hours). This could be influenced by the decision to calculate the maximum depth and conductivity for each calendar day; a single diurnal peak could be counted twice at the lower gauge (once for a given day at 11:30pm and once for the next day at 12:00am). Future research could mitigate this potential source of error by defining a "day" as starting at 12:00pm, as that time had almost no recorded peaks in discharge or conductivity and that would allow each diurnal cycle to be isolated.

If the difference in timing is caused by a single diurnal wave that travels downstream from the upstream gauge, then this would suggest that the wave celerity is 0.75 km/hr, based on the 5.25 km distance between the gauges and the 7-hour difference in timing. Converting from wave celerity to streamflow velocity suggests baseflow stream velocities around 0.1 to 0.2 m/s.

Discussion

For the summer months, both stream gauges indicated a decline in stream discharge and an increase in conductivity, with the upper gauge recording greater conductivity than the lower gauge until mid-July. Prior research in alpine environments found that ET and melting events drive summer diurnal cycles in small streams (Mutzner et al. 2015), and that the decline in snowmelt contributions leads to an overall decline in

stream discharge throughout the summer (Jencso et al. 2009). It is likely that snowmelt contributes to Horseshoe Creek's discharge throughout May and that as the snowmelt declines, ET further limits the amount of water that reaches the stream. The increase in cumulative ET throughout the summer corresponds well with the increase in conductivity (Figure 22), further supporting the idea that ET is the primary driving factor influencing the stream depth and conductivity in the summer months. ET's influence on streamwater thus extends beyond diurnal cycles to the seasonal timescale.

The upper gauge's higher conductivity indicates that the lake has higher conductivity and longer residence times compared to the hillslope, which aligns with other research that found significant contributions from lake water to discharge and conductivity at upstream gauges, with this effect waning downstream (Leach et al. 2017). In mid-July, the hillslope's conductivity likely increases enough that it becomes greater than the lake's, as that is when the lower gauge's conductivity becomes greater than the upper gauge's. This may be due to cumulative ET concentrating the groundwater on the hillslope and intercepting any low-conductivity rainwater, whereas the lake may receive some rainwater throughout the season.

The seasonal patterns, where stream depth and electrical conductivity are negatively correlated, are contrary to the diurnal patterns where stream depth and conductivity are directly correlated. The two tend to increase and decrease together, which is a pattern that can be caused by shallow lateral flow flushing solutes from the soil (Knapp et al. 2020). This supports the hypothesis that there are limited periods of hillslope-stream connectivity where the ion-rich shallow lateral flow is able to reach the stream, and during other periods the flow is intercepted by ET. In addition, if the stream

discharge was solely influenced by precipitation input and direct ET interception from the riparian zone, we would expect the maximum to occur around 10 am on days with no interference from precipitation (Gribovszki et al. 2008). This also implies that other mechanisms, such as groundwater travel time, are influencing the time of maximum water depth. During the day, marsh plants take up lake water and trees intercept shallow groundwater on its way to the stream during maximum ET, but these plants do not take up as much water overnight, allowing a pulse of water from the lake and shallow groundwater to enter the stream. The travel time of the groundwater through the soil and the surface water through the lake-wetland system could cause the pulse of water to reach the upper stream gauge later the following day and the lower stream gauge 6 hours after that.

I originally hypothesized that the diurnal response would primarily occur where vegetation grows close to the stream channel, limiting the direct effect to the upper catchment and leaving the lower stream gauge to lag behind the upper. However, when the rating curves were finalized, we found that the discharge at the upper gauge is approximately 10% of the discharge at the lower gauge. In addition, further investigation indicated that there are wetlands in the flatter area of the lower catchment (Figure 17b). The lower catchment likely experiences its own groundwater response, as the upper catchment contributions account for 10% of the lower gauge's streamflow, which is likely not enough to be the sole factor causing the diurnal cycles at the downstream gauge. The lower catchment's diurnal cycle could be partly due to hillslope groundwater contributions, or the upper gauge's conductivity signal traveling downstream, but the most likely hotspot for ET interception is at the noted wetlands (Figure 17). These plants

could intercept slow-moving stream and surface water, and increase the electrical conductivity of the remaining water via evaporative concentration. This aligns most with other studies, which have found that vegetation in the riparian zone has a direct influence on streamflow, while other vegetation farther from the stream has a lesser impact (Boronina et al. 2005; Gribovszki et al. 2010).

In precipitation-dominated systems, we expect conductivity to decrease when discharge does as the low-conductivity precipitation enters the stream (Knapp et al. 2020). Horseshoe Creek has the opposite relationship on the diurnal scale, where discharge and conductivity increase at the same time. These patterns could be created by a system where the inputs to the stream are higher conductivity than the stream baseflow is, and these inputs undergo evaporative concentration over time. In effect, high-conductivity lake water, groundwater, and shallow lateral flow could be intercepted by ET during the day, but as these waters enter the stream in the evening and overnight, they increase the stream's discharge and conductivity. Over the ET season, ET draws upon these waters, limiting the amount that reaches the stream and increasing the conductivity of what's left.

An additional factor influencing the streamflow is the varying lag times from high-conductivity sources such as the lake and wetland which are located in the upstream region and form the primary headwaters of Horseshoe Creek. These sources had the highest conductivities that we observed in the watershed, so varying outflow from these sources due to ET or other factors, in addition to variations in local shallow lateral flow, may influence the conductivity of the water carried in the stream channel. This relationship between discharge and electrical conductivity implies that the catchment is

dominated by groundwater and ET processes, especially as biological products in the organic horizon of the soil are a major source of conductivity for the shallow lateral flow.

These analyses are exploratory and could guide future research to test the hypotheses presented as explanations for the seasonal and diurnal cycles in streamflow and conductivity. Further investigation in the watershed could focus on other times of the year, as this study focused on summer months. This could include factors such as the timing of the spring groundwater maximum relative to the streamflow maximum: if the stream is fed by snowmelt traveling overland, the peak stream depth will occur before the groundwater table rises, but if the groundwater table is recharged first and then feeds the stream, groundwater will peak first. Any differences in timing of spring streamflow maxima between the two gauges could also imply differences in stream source; if the lower catchment is dominated by shallow lateral flow, its stream depth will likely peak either before the upper catchment's (if the upper is fed by deeper groundwater flow during spring melt), or after the upper catchment's (if the upper is fed by overland flow). More investigation into diurnal cycles could include analyses of the timing of minimum depth and conductivity, and any changes in lag time between the upper and lower gauges.

Other research could calculate the percent of streamflow that is attributed to subsurface hillslope flow by performing additional hydrograph separation, with the lower gauge as the one endmember and the upper gauge as the other endmember. This calculation would allow the comparison of lake outflow conductivity and hillslope conductivity, and it could investigate the hypothesis that the lower gauge's conductivity becomes higher than the upper gauge's in July due to the hillslope contributions' conductivity becoming greater than the lake contributions' conductivity.

Conclusions

1. ET and snowmelt drive seasonal stream cycles. Both the upper and lower stream gauges show seasonal patterns in stream depth and conductivity that could be explained by evapotranspiration intercepting and concentrating water inputs to the stream. The seasonal decrease in stream depth leads to an annual minimum in late August that coincides with the summer ET maximum and the hillslope groundwater minimum, further supporting that this streamflow pattern is due to ET's influence on source waters such as the lake and the hillslope soil water.

2. The seasonal increase in stream baseflow conductance over the summer months corresponds well to seasonal increase in cumulative ET ($R^2 = 0.947$, Figure 22). Evaporative concentration is the likely mechanism causing the seasonal increase in baseflow conductance. Root exudates and decomposition products are other sources of conductivity that likely contribute to streamflow conductivity, especially at the downstream gauge which receives inputs from the hillslope via subsurface pathways. The downstream gauge shows a greater increase in conductivity than the upstream gauge does, indicating that the hillslope is more heavily impacted by evaporative concentration and the addition of solutes than the lake is.

3. Diurnal variations are present in both streamflow and conductance, and the two factors tend to be correlated on this timescale. Maximum streamflow and conductance coincide at both gauges, with the upper gauge's maximum at 5 pm and the downstream gauge's maximum at midnight. ET is the only diurnally-variable factor studied that could influence streamflow, and it likely concentrates and intercepts both lake and hillslope source waters. The difference in timing between the two gauges could

be due to the travel time from the upstream gauge to the downstream gauge, if both gauges are recording one wave of highly conductive water traveling downstream. The timing difference could also be due to the lag time of water traveling through the lake and hillslope to the stream. Further research could investigate the lag times associated with water moving through the lake and hillslope, or it could further characterize the diurnal cycles by analyzing daily minima.

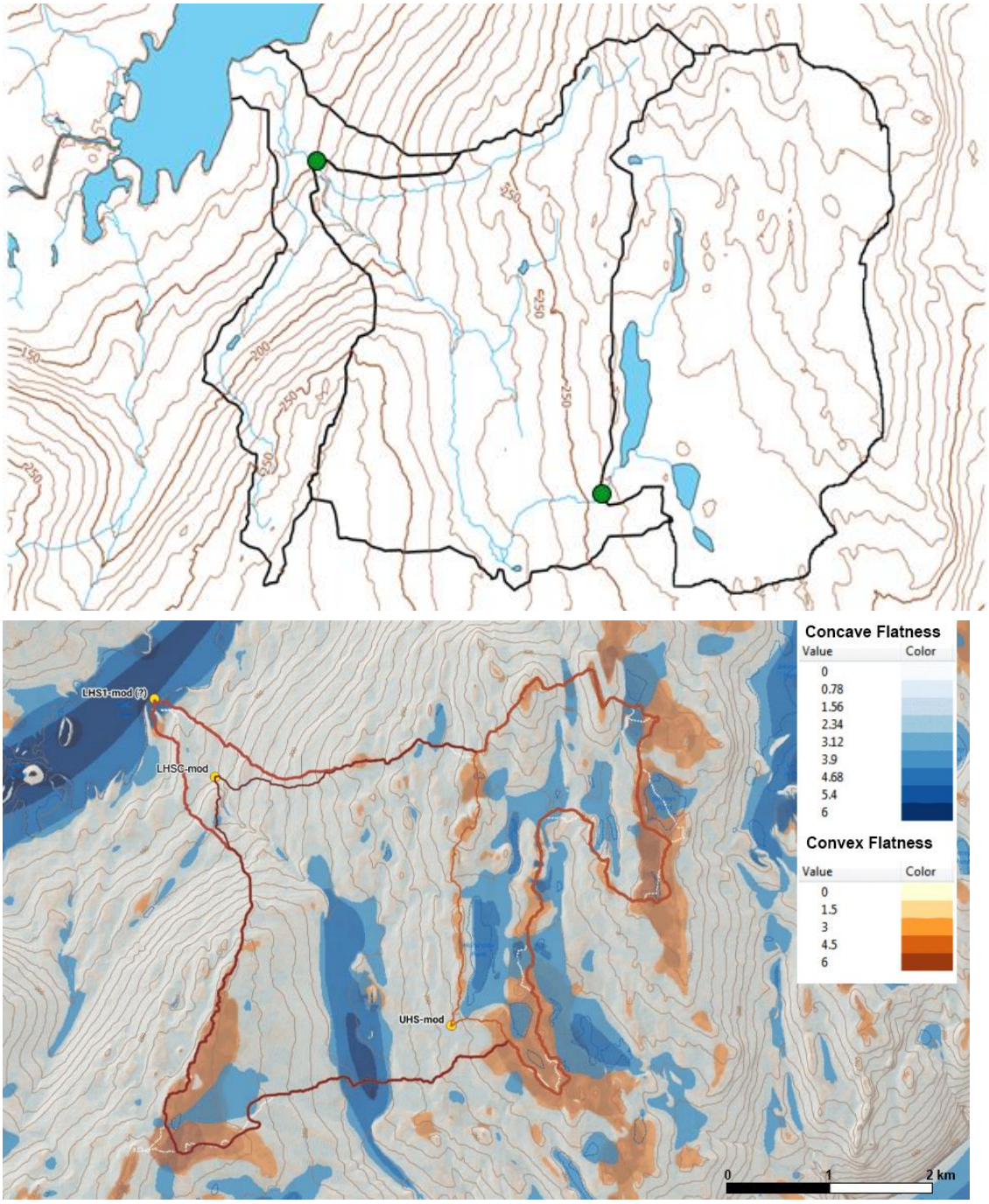

Figure 17. Top, contour map of Horseshoe Creek showing the two stream gauges (green dots), and demarcating the upper and lower basins (and the ungauged lowermost basin). Bottom, contour map of Horseshoe Creek showing where land is concave and convex. Note the flat topography and lakes in the upper basin, the steep hillslopes throughout the lower basin, and the concavely flat wetland area along the stream in the lower basin. Maps by Karen Prestegaard (top) and Sara Jenkins (bottom) using the Newfoundland GIS & Mapping Division's insular DEM (8 m resolution).

Figure 18. Top left, photo of Lower Horseshoe stream gauge. Right, photo looking down on Upper Horseshoe from road near gauge. Bottom left, the lake and wetland area that feeds in to Upper Horseshoe.

Table 3. Summary of Horseshoe Creek Watershed's water sources, their conductivities, and potential sources of the conductivity.

Water Sources	**Conductivity during ET season (µS/cm)**	**Source of Conductivity**
Shallow Flow (0-20 cm below surface)	30-70, increasing from May-August	Biological processes/leachates
Groundwater and Wetlands	5-50, increasing with water depth	Evaporative concentration, solutes
Stream	20-70, increasing from May-August	Inherited from water source
Lake	20-50	Snowmelt dilution, spring turnover, stratification, and evaporation
Precipitation	1.5 -3	Particles in the atmosphere or on snow

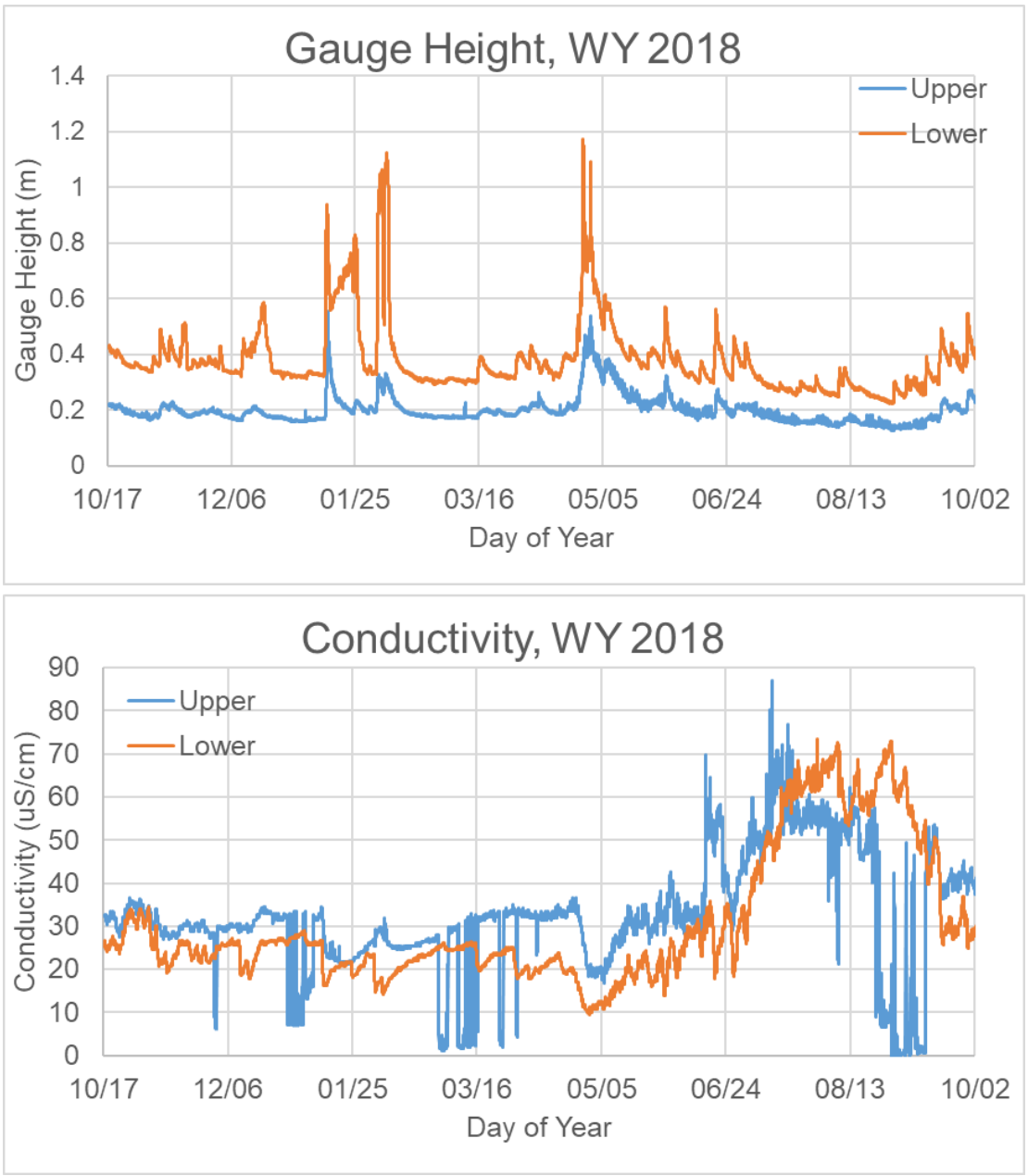

Figure 19. Graphs of gauge height and conductivity for the Upper and Lower Horseshoe gauges throughout WY 2018.

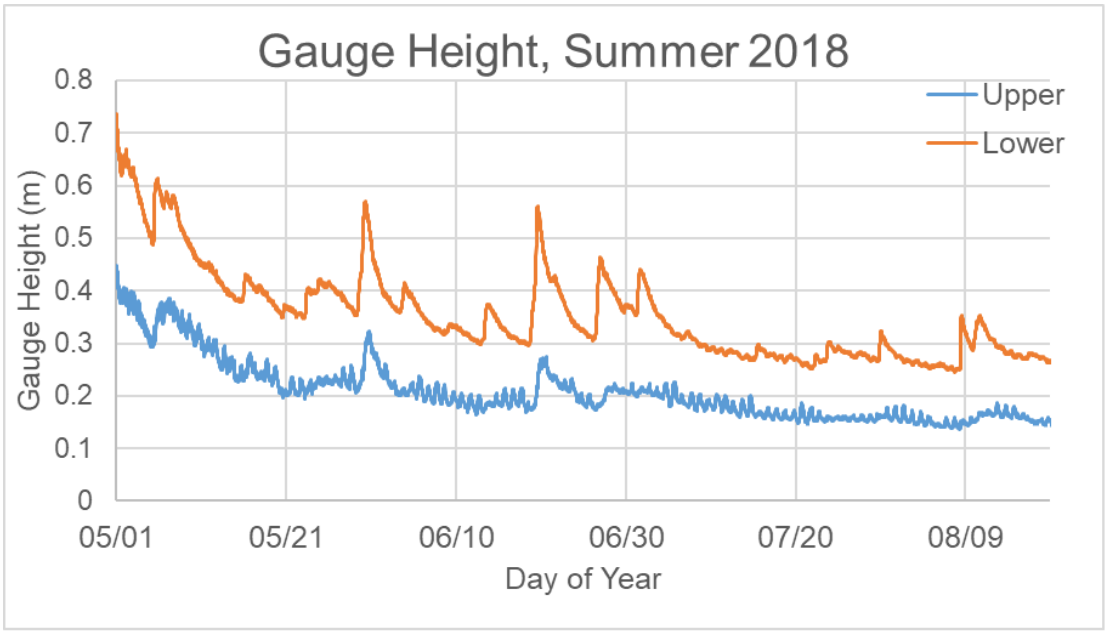

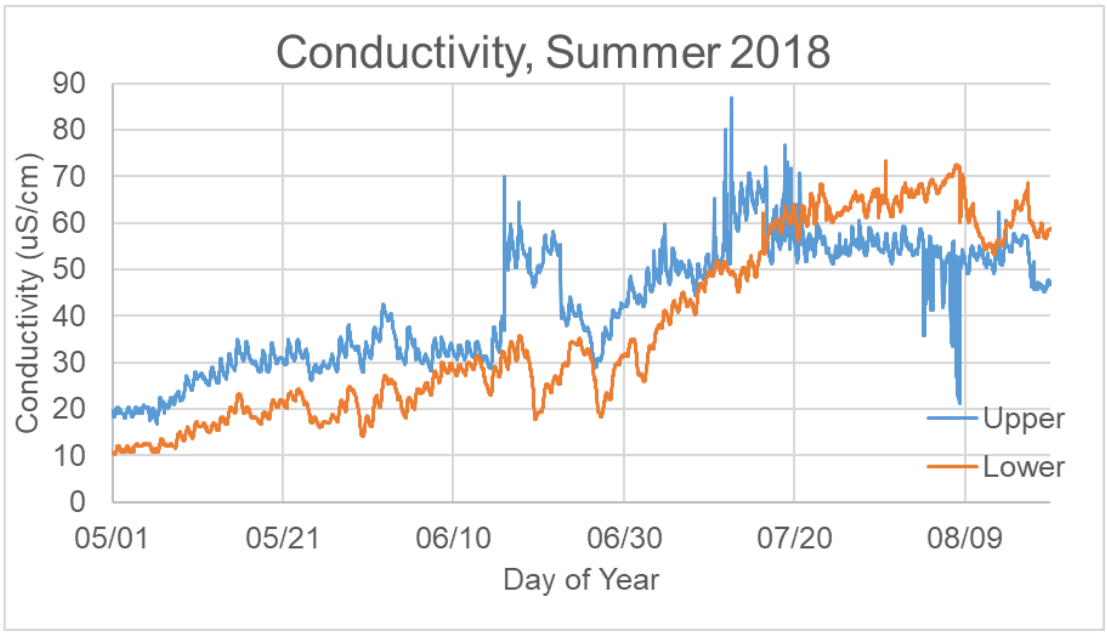

Figure 20. Graphs of gauge height and conductivity for the Upper and Lower Horseshoe gauges throughout summer 2018. Note the overall decrease in gauge height and the overall increase in streamflow at both gauges.

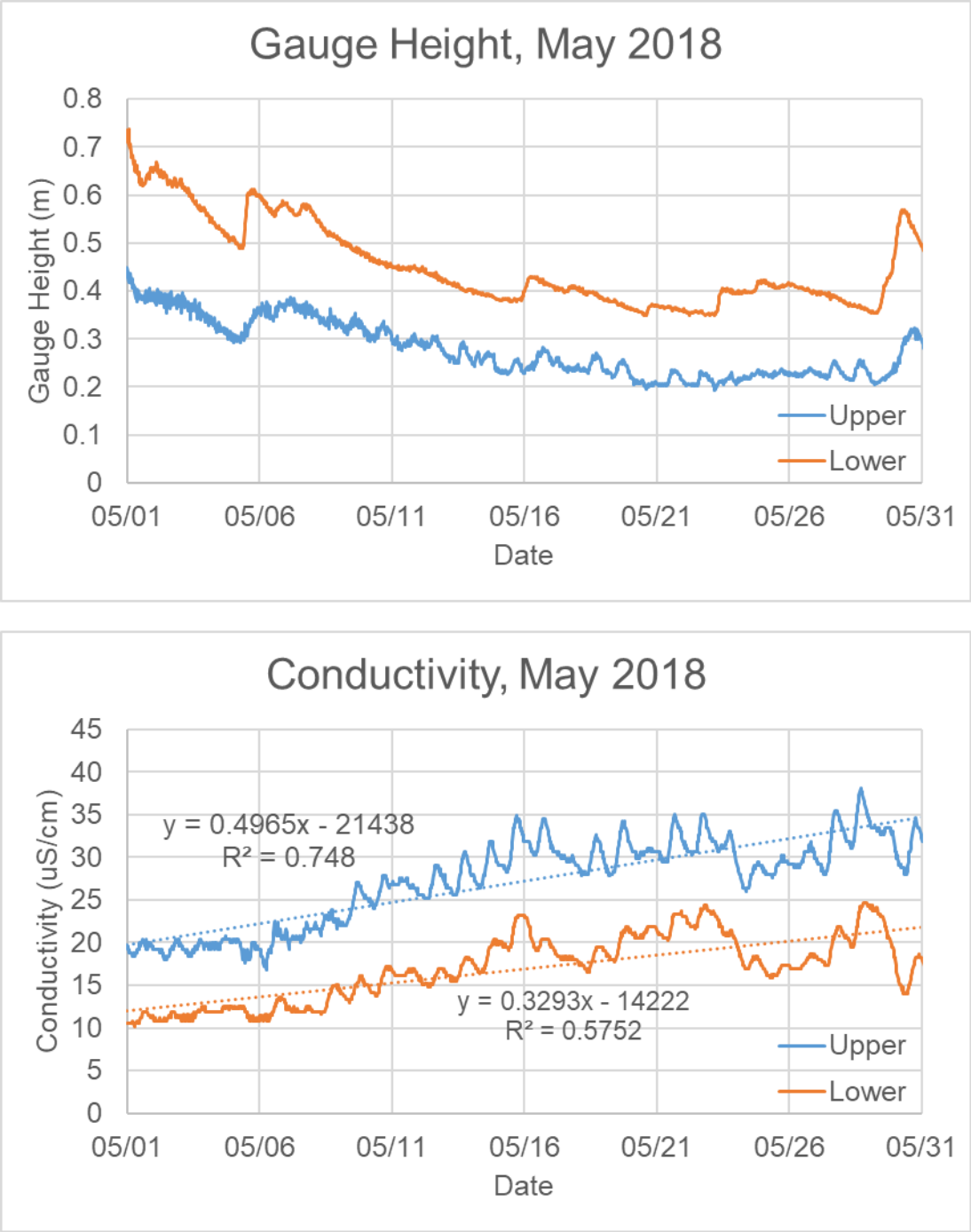

Figure 21. Graphs of gauge height and conductivity at the Upper and Lower Horseshoe gauging stations throughout May 2018. Note the larger diurnal variations and generally higher conductivity at the upper station, which is directly downstream of a lake.

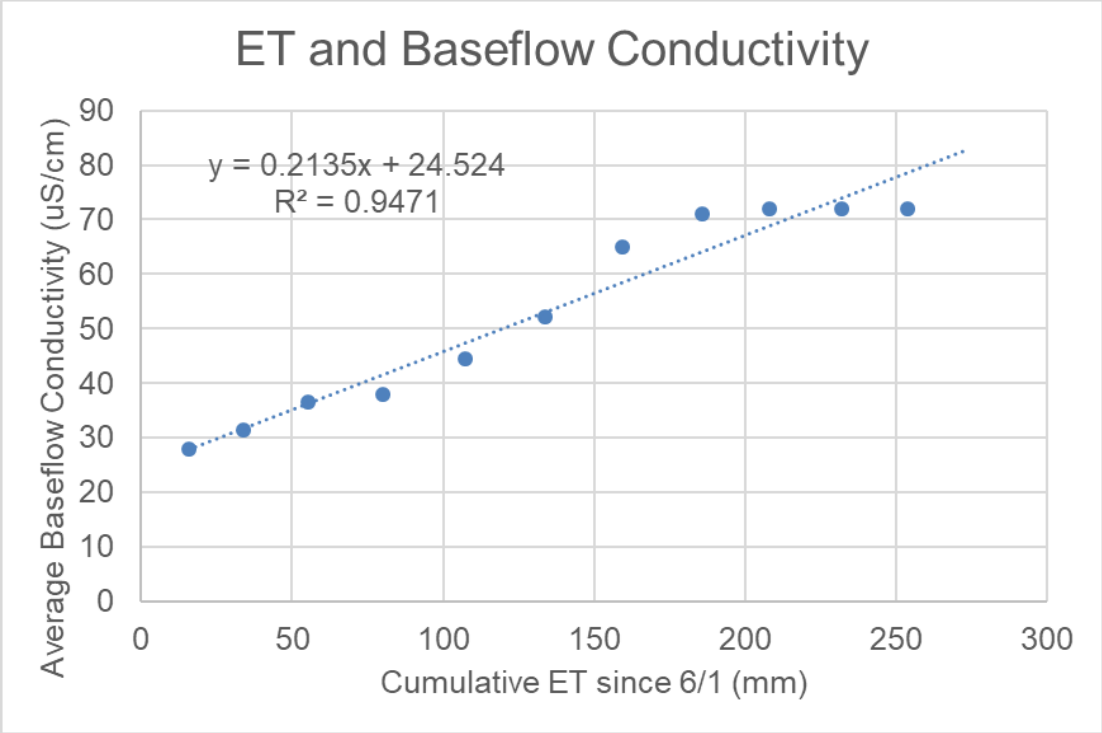

Figure 22. Average baseflow conductivity compared to cumulative ET. Baseflow conductivity was averaged over 8-day periods to correspond to the 8-day ET data. ET was averaged over multiple years as in Figure 13.

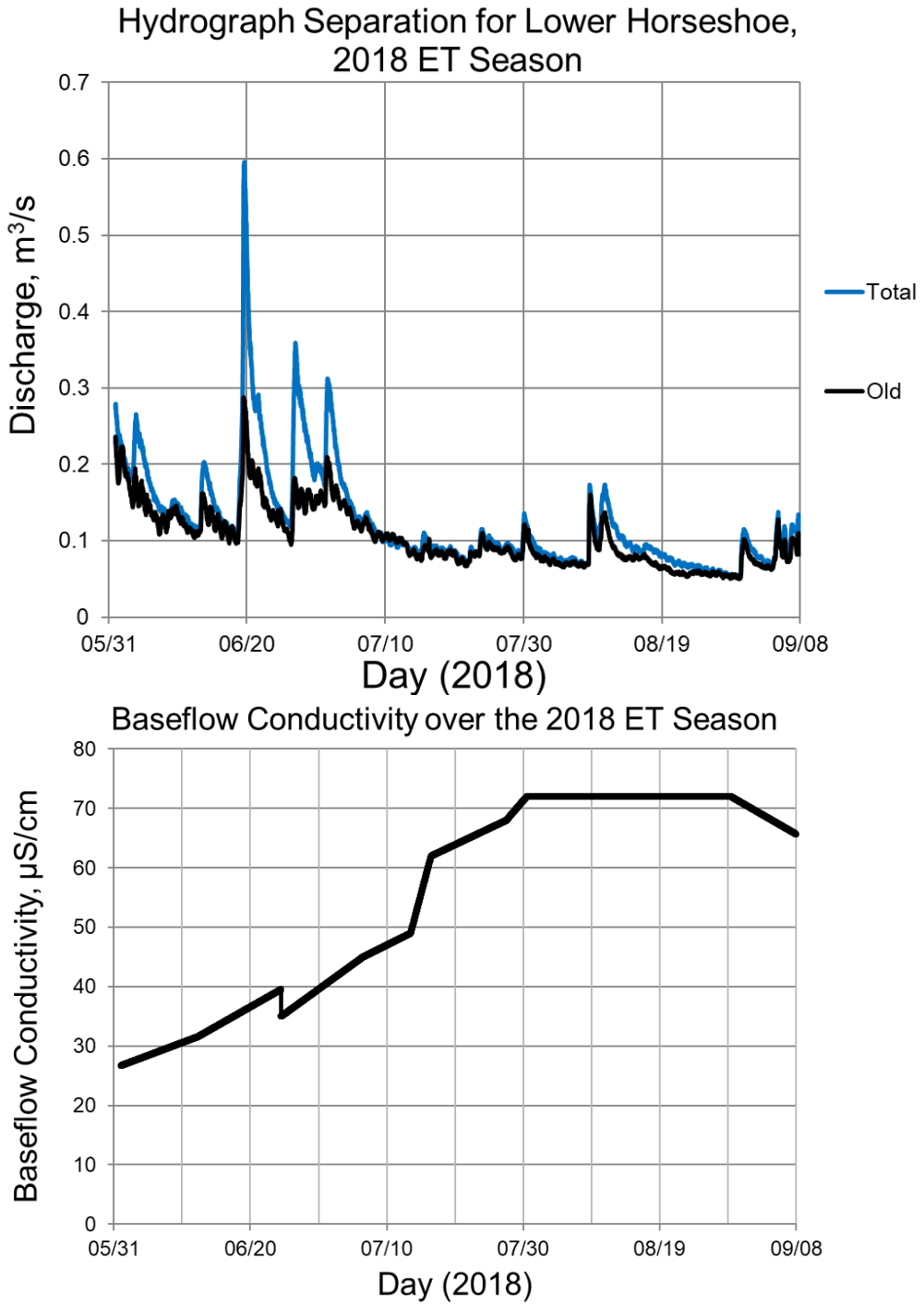

Figure 23. Top, hydrograph separation for the Lower Horseshoe gauging station, calculated by Karen Prestegaard using a low-conductivity endmember (precipitation, 1.5 µS/cm) and a changing high-conductivity endmember (baseflow, 25-71 µS/cm). Bottom, baseflow electrical conductivity calculated by Karen Prestegaard, informed by the increase in measured conductivity of stream and water samples over the ET season.

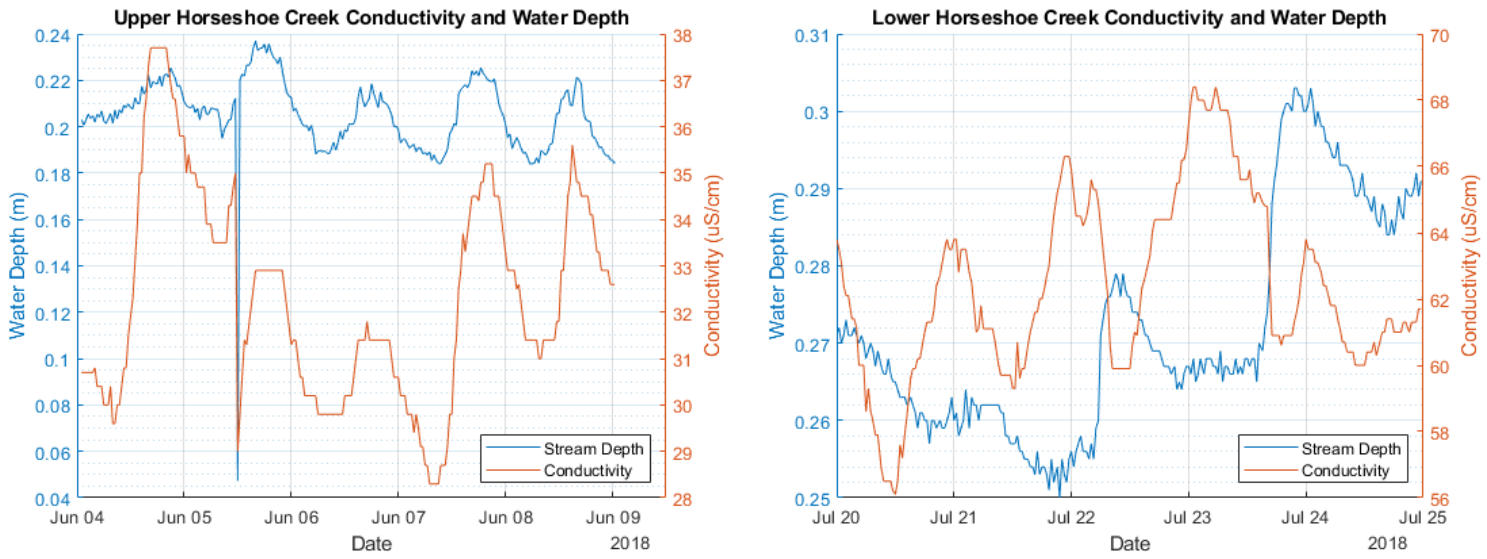

Figure 24. Stream depth and conductivity over 5-day periods from the ET season of 2018 at each of the gauges. Gauge height and conductivity both undergo daily cycles at each gauge. Different time periods were chosen to minimize precipitation interference; a small (3-mm) precipitation event on 6/3/18 did not appear to affect the upper gauge but the lower gauge showed increased depth and no diurnal cycle through June 8, and another event on 7/24/18 interfered with the upper gauge's cycle but not the lower gauge's.

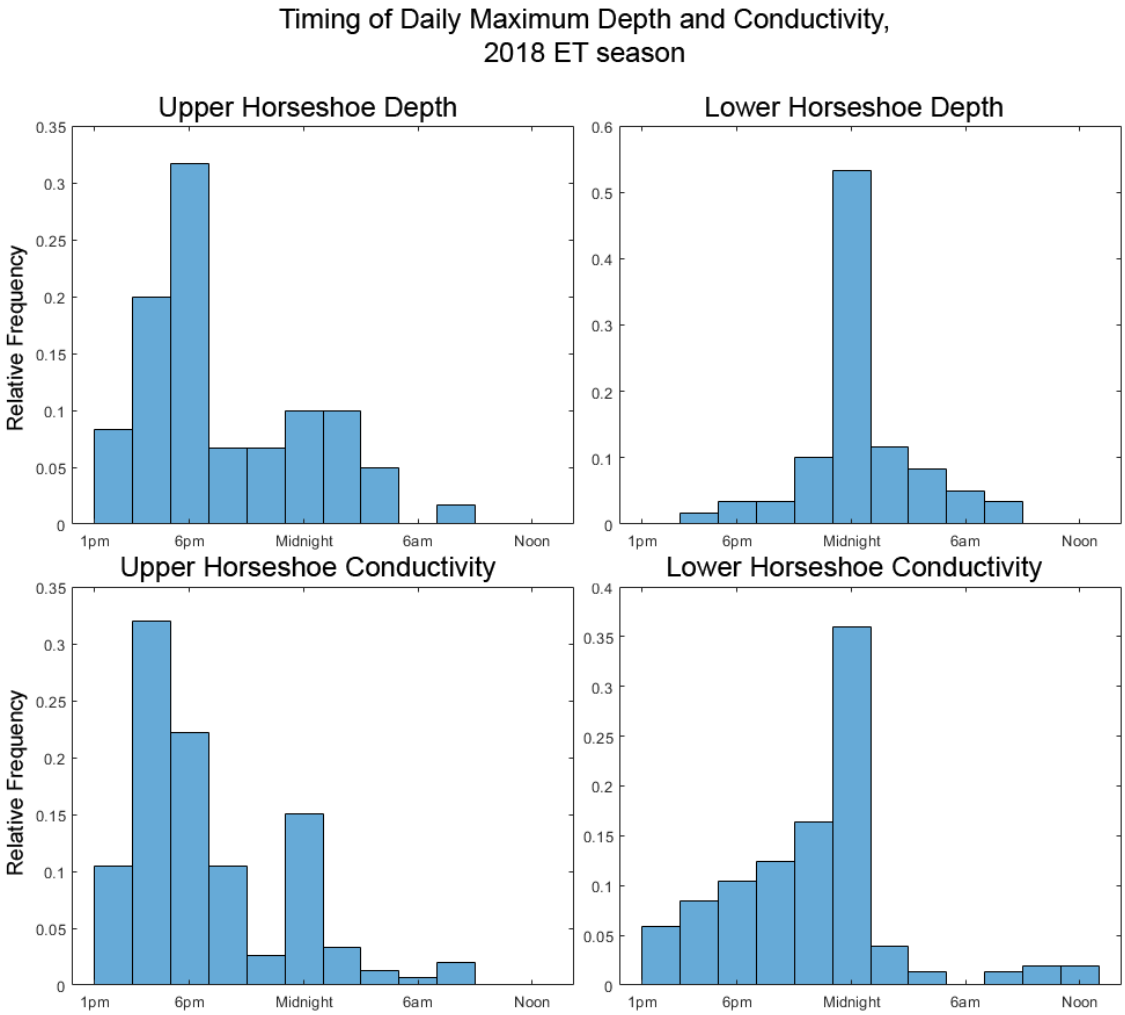

Figure 25. Histograms showing timing of daily maximum depth and conductivity at the Upper and Lower Horseshoe gauging stations for the ET period of 2018. Note that the depth and conductivity at each gauge generally occur at the same time: 3-7 pm for Upper Horseshoe, and 11 pm-1 am for Lower Horseshoe.

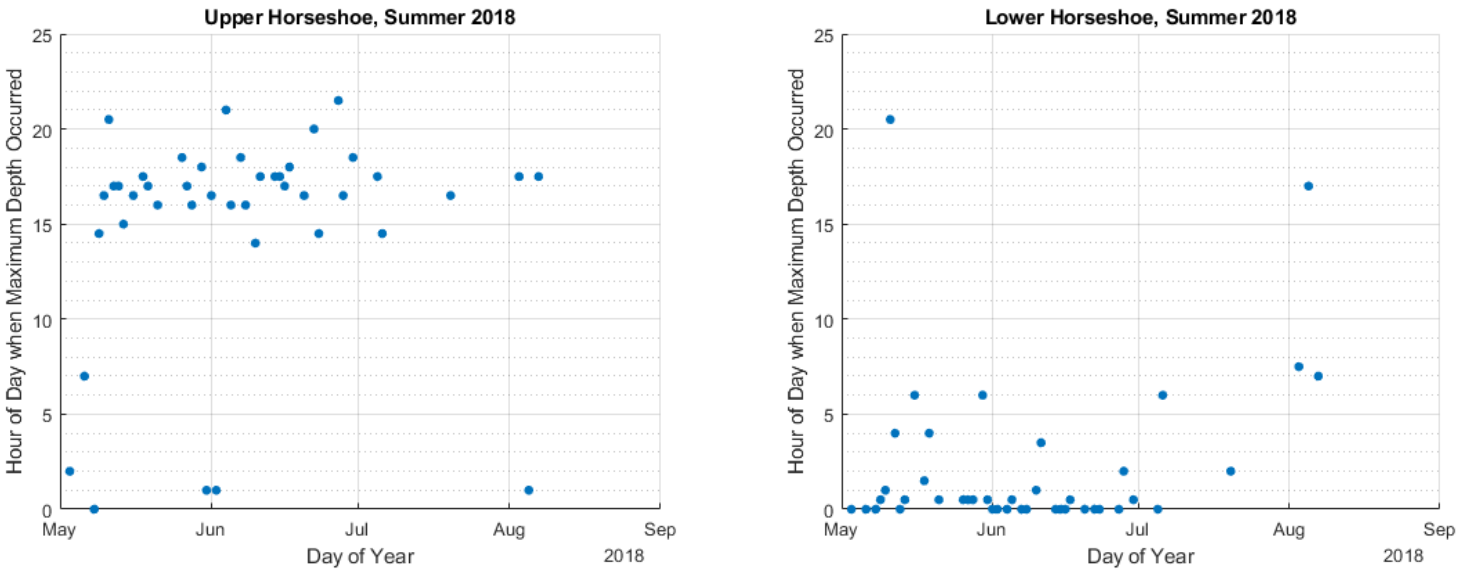

Figure 26. Scatterplots of the timing of daily maximum depth for Upper and Lower Horseshoe gauging stations.

Chapter 4: Implications and Conclusions

The hydrology of Horseshoe Creek Catchment is heavily influenced by and linked to plant transpiration, on multiple spatial and temporal scales. On the hillslope, seasonal cycles are visible in the groundwater depth distribution. Upper soil layers have the highest water flux, as infiltrating precipitation is quickly taken up by trees and moss for transpiration. Much of the remaining water flows laterally downslope due to the hydraulic conductivity contrast between the organic soil horizon and the mineral soil. Throughout the warmer months, ET forces the groundwater table decline as trees primarily intercept inflow and prevent the groundwater table from recharging, and secondarily access groundwater directly with the small proportion of deep roots that the trees grow. ET is then limited by shallow soil water availability, which is dependent on precipitation, specific yield, and lateral flow rates.

On the catchment scale, ET drives a seasonal decrease in streamflow and increase in conductivity. It removes water from the lake and hillslope, concentrating the remaining water and reducing the total amount of water that reaches the stream from these sources. Diurnal cycles show conductivity and streamflow peaking in the evening at the upper gauge and overnight at the lower gauge. For the lower catchment, daytime ET limits the hillslope contribution to the stream, cutting off this source during times when ET is active. When ET lessens overnight, water can flow laterally through the upper soil layers, picking up ions so that the stream receives a pulse of water with high electrical conductivity. Plants growing in wetlands and lakes also increase electrical conductivity of the stream water, especially in the upper catchment, by removing some

water for their transpiration and concentrating the remaining water. Finally, plants in the catchment also influence stream electrical conductivity by their root exudates and decomposition byproducts. These chemicals are a source of ions in the organic horizon, which are mobilized by lateral flow and carried to the stream. The hydrologic processes in this boreal forest are thus closely related to plant transpiration, root structure, and soil structure.

As this boreal forest is expected to warm with global climate change (Wang et al. 2014), annual total ET may increase somewhat with the extended growing season. However, if there is only a slight increase in summer precipitation associated with this warming (Wang et al. 2014), summer precipitation may limit ET if sources of ET remain the same (i.e. similar tree root depths and densities). If this is the case, there would likely be extended periods during the growing season when ET exceeds precipitation. This increase in the summer precipitation used for ET may result in a decreased connectivity between the hillslope and the stream. Dissolved organic carbon fluxes would likely then become more variable throughout the year, with very low fluxes in the summer as shallow lateral flow is limited, and much higher fluxes in the early fall as lateral flow picks up soil organic carbon that has built up over the summer (Tranvik et al. 2009).

Trees may also have to invest in accessing deeper groundwater during the summer, especially near tops of hillslopes that lose water to both ET and drainage. This additional root investment would require more metabolic effort be put into growing deep roots. This would limit the amount of excess energy that trees could direct into developing wider root systems or growing more branches and needles, which may generate a negative feedback, thus limiting how much additional ET the trees can

produce. This may put native *Picea* trees at a competitive disadvantage with northward invading temperate-forest tree species, as temperate forests tend to have deeper water tables than boreal forests (Fan et al. 2017) and trees native to these forests likely have roots and root structures that are better suited to accessing deep water tables. Downslope locations may experience an even more dramatic decline in seasonal water table compared to upslope locations, as increased ET upslope intercepts more lateral flow that would have contributed to downslope groundwater, and increased ET downslope more directly intercepts groundwater recharge. Overall, there will likely be changes in trees' behavior, in annual ET amount, and in tree species diversity, which will change the hillslope and catchment hydrology of Horseshoe Creek.

As important SOC sinks (Angstmann et al. 2012; Scharlemann et al. 2014; Ziegler et al. 2017), the impact of climate change on boreal forests worldwide could further exacerbate global warming. This maritime boreal forest will likely be less heavily impacted by climate change compared to Canadian continental boreal forests, as the maritime boreal forest is expected to experience a slight increase in annual precipitation while the continental forests are predicted to experience heavy drying (Wang et al. 2014). However, the maritime boreal forest will still be changed by global warming, and these changes could be magnified by the interactions between ET, rooting depths, soil characteristics, and hydrologic processes. It is essential to further investigate these factors and the relationships among them to fully evaluate how this boreal ecosystem will respond to climate change.

Appendix A: Matlab Code

```
%% Code to find daily maximum depth and the time at which it occurs (can be modified for conductivity, etc)
clear; close all

%% Load data into matrix
opts = detectImportOptions('LHdepth.csv') ; % reference csv file with date/time in column 1 and water depth in column 2
opts.DataLines = [2,18236] ; % exclude first row, which has labels and no data
rawdata = readtable('LHdepth.csv',opts) ; % load data into matlab table
LHdepth = rawdata(:, 1:2) ; % copy data into new table
LHdepth.Day = dateshift(LHdepth.Var1,'start','day') ; % make new column with day but no time
LHdepth.Properties.VariableNames = {'Time','X','Day'} ; % rename columns

%% Run function to find daily maxes
maxinfo =
rowfun(@maxDepthFunction,LHdepth,'GroupingVariable','Day','OutputVariableNames',
{'MaxTime' 'MaxX'});
% make table with all the max depth/time data, using function described at the end of this script
% col1=day, col2=#number of data points on that day,
% col3=time of max depth, col4=max depth

%% Function to find max depth/time
function [tmax,xmax] = maxDepthFunction(t,x) % return maximum depth (x) and time where that occurs (t)
[xmax,imax] = max(x,[],1);
tmax = t(imax);
end
```

Appendix B: Root Measurements

Table B1. Measured root lengths and diameters for upslope soil pits, organized by soil pit and layer. Volume was calculated using measured diameter and length, and assuming roots were cylindrical, such that $V=\pi(d/2)^2L$.

Soil Pit and Layer	Diameter (cm)	Length (cm)	Volume (cm^3)
U-1 Moss	0.1	52.5	0.4
	0.1	31.0	0.2
	0.2	33.9	1.1
	0.2	18.6	0.6
	0.2	38.1	1.2
	0.3	25.7	1.8
	0.3	39.6	2.8
	0.3	20.0	1.4
	0.3	48.7	3.4
	0.4	35.3	4.4
	0.4	20.5	2.6
	0.4	28.5	3.6
	0.4	50.4	6.3
	0.4	33.4	4.2
	0.4	13.3	1.7
	0.4	42.8	5.4
	0.4	62.9	7.9
	0.4	104.7	13.2
	0.4	18.6	2.3
	0.5	40.6	8.0
	0.5	43.1	8.5
	0.5	48.2	9.5
	0.5	75.8	14.9
	0.6	66.4	18.8
	0.6	94.4	26.7
	0.6	98.3	27.8
	0.6	21.5	6.1
	0.6	18.2	5.1
	0.6	15.4	4.4
	0.7	23.3	9.0
	0.7	12.8	4.9
	0.8	47.7	24.0
	0.8	100.4	50.5
	0.8	66.2	33.3
	0.9	38.1	24.2
	1.1	59.8	56.8
	1.1	34.5	32.8
	1.3	76.4	101.4
	1.3	93.0	123.4
	1.3	89.8	119.2

Table B2. Measured root lengths and diameters for downslope soil pits, organized by soil pit and layer. Volume was calculated using measured diameter and length, and assuming roots were cylindrical, such that $V=\pi(d/2)^2L$.

Soil Pit and Layer	Diameter (cm)	Length (cm)	Volume (cm^3)
D-1 Moss	0.3	19.6	1.4
	0.3	22.7	1.6
	0.3	9.2	0.7
	0.3	17.2	1.2
	0.3	10.5	0.7
	0.3	30.7	2.2
	0.3	29.1	2.1
	0.3	25.2	1.8
	0.3	48.2	3.4
	0.3	33.2	2.3
	0.3	25.4	1.8
	0.3	24.2	1.7
	0.3	28.6	2.0
	0.3	24.2	1.7
	0.3	78.6	5.6
	0.3	55.4	3.9
	0.3	19.6	1.4
	0.4	18.4	2.3
	0.4	21.1	2.7
	0.4	18.6	2.3
	0.4	6.4	0.8
	0.4	20.2	2.5
	0.4	5.3	0.7
	0.4	75.7	9.5
	0.4	31.4	3.9
	0.4	55.2	6.9
	0.4	18.7	2.3
	0.4	42.6	5.4
	0.4	46.2	5.8
	0.4	8.5	1.1
	0.4	14.9	1.9
	0.4	58.3	7.3
	0.5	24.3	4.8
	0.5	21.4	4.2
	0.5	41.3	8.1
	0.5	23.8	4.7
	0.5	6.8	1.3
	0.5	42.7	8.4
	0.5	91.3	17.9
	0.5	14.7	2.9

	1.4	41.4	63.7
	1.4	32.5	50.0
	1.4	30.2	46.5
	1.5	73.2	129.4
	3.4	86.3	783.5
U-1 Organic	0.2	34.9	1.1
	0.3	20.2	1.4
	0.3	23.3	1.6
	0.3	46.8	3.3
	0.3	26.8	1.9
	0.3	21.0	1.5
	0.3	35.6	2.5
	0.3	15.2	1.1
	0.3	10.1	0.7
	0.3	25.1	1.8
	0.3	23.2	1.6
	0.3	26.5	1.9
	0.4	21.6	2.7
	0.4	55.6	7.0
	0.4	36.0	4.5
	0.4	16.7	2.1
	0.4	73.2	9.2
	0.4	14.7	1.8
	0.4	23.8	3.0
	0.4	42.3	5.3
	0.4	30.2	3.8
	0.4	23.5	3.0
	0.4	11.2	1.4
	0.4	18.4	2.3
	0.4	17.1	2.1
	0.4	20.7	2.6
	0.4	16.5	2.1
	0.4	16.5	2.1
	0.4	23.4	2.9
	0.4	26.9	3.4
	0.4	11.0	1.4
	0.4	27.8	3.5
	0.4	18.2	2.3
	0.4	17.9	2.2
	0.4	5.7	0.7
	0.5	66.4	13.0
	0.5	54.6	10.7
	0.5	40.3	7.9
	0.5	16.6	3.3
	0.5	16.7	3.3
	0.5	33.9	6.7
	0.5	13.8	2.7
	0.5	21.8	4.3
	0.5	25.4	5.0
	0.5	12.5	2.5
	0.5	5.6	1.1
	0.6	34.5	9.8

	0.5	101.8	20.0
	0.5	4.7	0.9
	0.6	6.6	1.9
	0.6	22.2	6.3
	0.6	18.7	5.3
	0.6	71.2	20.1
	0.6	85.8	24.3
	0.6	57.7	16.3
	0.6	34.8	9.8
	0.6	53.6	15.2
	0.6	22.3	6.3
	0.6	24.0	6.8
	0.6	10.2	2.9
	0.6	11.2	3.2
	0.7	13.4	5.2
	0.7	6.2	2.4
	0.7	37.5	14.4
	0.7	40.1	15.4
	0.7	41.2	15.9
	0.7	65.7	25.3
	0.7	82.4	31.7
	0.7	41.8	16.1
	0.7	8.3	3.2
	0.7	13.4	5.2
	0.7	6.3	2.4
	0.8	22.4	11.3
	0.8	19.2	9.7
	0.9	15.1	9.6
	0.9	13.6	8.7
	0.9	11.1	7.1
	0.9	25.2	16.0
	0.9	16.4	10.4
	0.9	30.2	19.2
	0.9	9.9	6.3
	0.9	8.7	5.5
	1.0	8.9	7.0
	1.0	26.1	20.5
	1.0	31.9	25.1
	1.0	76.5	60.1
	1.1	24.7	23.5
	1.1	19.2	18.2
	1.1	18.6	17.7
	1.1	8.4	8.0
	1.2	29.0	32.8
	1.2	11.5	13.0
	1.3	11.6	15.4
	1.3	29.8	39.6
	1.3	18.6	24.7
	1.3	10.5	13.9
	1.4	15.0	23.1
	1.5	80.5	142.3
	1.5	17.1	30.2
	1.5	6.9	12.2

	0.6	28.9	8.2
	0.6	28.6	8.1
	0.6	27.3	7.7
	0.6	36.8	10.4
	0.6	31.0	8.8
	0.6	23.9	6.8
	0.6	23.0	6.5
	0.6	17.3	4.9
	0.6	19.1	5.4
	0.6	19.7	5.6
	0.6	16.7	4.7
	0.6	6.2	1.8
	0.6	15.7	4.4
	0.6	8.0	2.3
	0.6	6.8	1.9
	0.6	24.3	6.9
	0.6	23.9	6.8
	0.6	15.0	4.2
	0.6	24.6	7.0
	0.6	7.6	2.1
	0.6	11.1	3.1
	0.6	7.0	2.0
	0.7	46.7	18.0
	0.7	8.8	3.4
	0.7	8.5	3.3
	0.7	31.1	12.0
	0.7	30.1	11.6
	0.7	7.6	2.9
	0.7	8.2	3.2
	0.7	5.6	2.2
	0.7	10.6	4.1
	0.7	17.5	6.7
	0.7	7.0	2.7
	0.7	3.3	1.3
	0.8	29.1	14.6
	0.8	58.2	29.3
	0.8	14.4	7.2
	0.8	17.8	8.9
	0.8	32.5	16.3
	0.8	14.6	7.3
	0.8	8.0	4.0
	0.9	48.2	30.7
	0.9	90.7	57.7
	0.9	22.8	14.5
	0.9	18.0	11.5
	0.9	9.4	6.0
	0.9	6.9	4.4
	0.9	3.5	2.2
	1.0	47.1	37.0
	1.0	39.6	31.1
	1.1	28.7	27.3
	1.2	67.8	76.7
	1.2	17.4	19.7

	1.5	30.4	53.7
	1.7	45.5	103.3
	1.8	33.3	84.7
	1.9	41.4	117.4
	1.9	36.4	103.2
	2.0	33.0	103.7
	2.1	20.7	71.7
	2.3	91.4	379.7
	2.3	15.6	64.8
	2.4	55.0	248.8
	2.8	63.3	389.8
	3.7	71.4	767.7
D-1 Organic	0.3	51.4	3.6
	0.3	30.8	2.2
	0.3	19.0	1.3
	0.3	34.8	2.5
	0.3	41.4	2.9
	0.3	47.2	3.3
	0.4	37.8	4.8
	0.4	47.2	5.9
	0.4	19.0	2.4
	0.4	14.3	1.8
	0.4	15.7	2.0
	0.4	48.4	6.1
	0.5	13.1	2.6
	0.6	7.9	2.2
	0.6	13.8	3.9
	0.6	20.4	5.8
	0.6	5.2	1.5
	0.7	37.8	14.5
	0.7	17.8	6.9
	0.7	8.6	3.3
	0.8	22.3	11.2
	0.8	4.5	2.3
	0.8	10.2	5.1
	0.9	29.8	19.0
	0.9	5.3	3.4
	0.9	4.8	3.1
	0.9	8.0	5.1
	1.1	7.0	6.7
	1.1	5.7	5.4
	1.2	25.4	28.7
	1.2	6.9	7.8
	1.5	10.5	18.6
	1.6	14.2	28.6
	1.7	27.6	62.6
	2.0	21.8	68.5
	2.6	92.4	490.6
	2.7	16.0	91.6
D-2 Moss	0.2	53.4	1.7
	0.2	31.4	1.0
	0.2	19.7	0.6

	1.3	29.9	39.7
	1.3	21.7	28.8
	1.3	18.4	24.4
	1.4	39.3	60.5
	1.6	7.0	14.1
	2.1	6.5	22.5
	2.2	46.2	175.6
U-1 Ae	0.3	29.4	2.1
	0.3	13.0	0.9
	0.3	19.8	1.4
	0.3	21.1	1.5
	0.3	6.5	0.5
	0.4	44.8	5.6
	0.4	51.1	6.4
	0.4	21.6	2.7
	0.4	21.4	2.7
	0.4	11.7	1.5
	0.4	11.9	1.5
	0.4	16.6	2.1
	0.4	16.7	2.1
	0.4	23.4	2.9
	0.4	5.9	0.7
	0.4	9.2	1.2
	0.4	21.1	2.7
	0.4	5.5	0.7
	0.4	12.1	1.5
	0.4	6.2	0.8
	0.4	21.7	2.7
	0.4	26.7	3.4
	0.4	12.0	1.5
	0.4	9.3	1.2
	0.4	4.2	0.5
	0.5	26.4	5.2
	0.5	6.0	1.2
	0.5	4.1	0.8
	0.5	19.0	3.7
	0.5	5.8	1.1
	0.5	11.3	2.2
	0.5	24.5	4.8
	0.5	3.3	0.6
	0.5	17.6	3.5
	0.5	13.5	2.7
	0.5	3.9	0.8
	0.5	5.7	1.1
	0.6	24.7	7.0
	0.6	15.2	4.3
	0.6	13.9	3.9
	0.6	8.2	2.3
	0.6	7.0	2.0
	0.6	11.1	3.1
	0.6	19.0	5.4
	0.6	6.5	1.8

	0.2	18.4	0.6
	0.3	23.2	1.6
	0.3	35.0	2.5
	0.3	29.1	2.1
	0.3	23.6	1.7
	0.3	30.9	2.2
	0.3	29.6	2.1
	0.3	9.6	0.7
	0.3	12.5	0.9
	0.3	5.6	0.4
	0.3	22.1	1.6
	0.3	8.8	0.6
	0.3	17.7	1.3
	0.3	9.4	0.7
	0.3	37.3	2.6
	0.3	32.2	2.3
	0.3	10.5	0.7
	0.3	24.4	1.7
	0.3	15.0	1.1
	0.3	71.0	5.0
	0.3	27.1	1.9
	0.3	24.3	1.7
	0.3	24.6	1.7
	0.3	37.5	2.7
	0.3	31.6	2.2
	0.3	17.6	1.2
	0.3	19.5	1.4
	0.3	43.4	3.1
	0.3	31.8	2.2
	0.3	99.1	7.0
	0.3	49.4	3.5
	0.3	60.0	4.2
	0.3	29.6	2.1
	0.3	44.5	3.1
	0.3	26.6	1.9
	0.3	8.3	0.6
	0.3	22.0	1.6
	0.3	36.6	2.6
	0.3	41.6	2.9
	0.3	10.9	0.8
	0.3	46.8	3.3
	0.3	23.7	1.7
	0.3	38.2	2.7
	0.3	12.8	0.9
	0.4	40.4	5.1
	0.4	23.1	2.9
	0.4	10.8	1.4
	0.4	27.0	3.4
	0.4	17.2	2.2
	0.4	38.2	4.8
	0.4	15.7	2.0
	0.4	64.1	8.1
	0.4	8.4	1.1

	0.7	32.4	12.5
	0.7	4.9	1.9
	0.7	8.8	3.4
	0.7	18.6	7.2
	0.7	4.1	1.6
	0.8	25.2	12.7
	0.8	38.3	19.3
	0.8	21.3	10.7
	0.8	24.4	12.3
	0.8	12.4	6.2
	0.8	22.6	11.4
	0.8	4.2	2.1
	0.9	16.3	10.4
	0.9	18.2	11.6
	0.9	16.6	10.6
	0.9	13.3	8.5
	0.9	3.7	2.4
	0.9	6.4	4.1
	0.9	10.0	6.4
	0.9	7.7	4.9
	0.9	11.2	7.1
	1.0	37.3	29.3
	1.0	11.2	8.8
	1.0	12.9	10.1
	1.0	10.2	8.0
	1.0	7.3	5.7
	1.0	10.2	8.0
	1.0	4.1	3.2
	1.0	6.5	5.1
	1.1	48.0	45.6
	1.1	26.3	25.0
	1.1	8.1	7.7
	1.2	12.4	14.0
	1.2	17.6	19.9
	1.2	4.5	5.1
	1.3	22.1	29.3
	1.4	18.4	28.3
	1.6	16.3	32.8
	1.7	55.0	124.8
	1.7	4.6	10.4
	1.7	7.9	17.9
	2.0	4.2	13.2
	2.1	8.2	28.4
	4.0	8.2	103.0
	5.8	31.4	829.6

	0.4	12.9	1.6
	0.4	16.7	2.1
	0.4	13.8	1.7
	0.4	19.1	2.4
	0.4	77.1	9.7
	0.4	26.5	3.3
	0.4	34.4	4.3
	0.4	24.8	3.1
	0.4	43.8	5.5
	0.4	25.2	3.2
	0.4	54.8	6.9
	0.4	25.2	3.2
	0.4	27.8	3.5
	0.4	28.4	3.6
	0.4	12.8	1.6
	0.4	10.1	1.3
	0.4	20.1	2.5
	0.4	21.0	2.6
	0.4	10.9	1.4
	0.4	13.8	1.7
	0.5	9.5	1.9
	0.5	19.9	3.9
	0.5	26.5	5.2
	0.5	11.8	2.3
	0.5	79.4	15.6
	0.5	28.7	5.6
	0.5	43.9	8.6
	0.5	21.4	4.2
	0.5	31.8	6.2
	0.5	6.4	1.3
	0.6	76.2	21.5
	0.6	23.1	6.5
	0.7	21.4	8.2
	0.8	63.3	31.8
	0.8	21.2	10.7
	0.9	71.2	45.3
	0.9	41.2	26.2
	1.1	10.3	9.8
	1.2	9.4	10.6
	1.3	83.2	110.4
	1.4	22.0	33.9
	1.6	24.2	48.7
	1.6	14.6	29.4
	1.7	85.2	193.4
	1.9	50.2	142.3
D-2 Organic	0.3	33.6	2.4
	0.3	27.9	2.0
	0.3	88.7	6.3
	0.3	22.1	1.6
	0.3	35.9	2.5
	0.3	14.2	1.0
	0.3	39.4	2.8

	0.4	44.9	5.6
	0.4	25.1	3.2
	0.4	15.2	1.9
	0.4	46.3	5.8
	0.4	26.2	3.3
	0.4	19.7	2.5
	0.4	20.8	2.6
	0.4	45.2	5.7
	0.4	16.6	2.1
	0.4	22.4	2.8
	0.4	27.0	3.4
	0.4	11.1	1.4
	0.4	18.6	2.3
	0.4	31.5	4.0
	0.4	27.2	3.4
	0.4	16.5	2.1
	0.4	12.3	1.5
	0.4	13.6	1.7
	0.4	9.5	1.2
	0.5	20.5	4.0
	0.5	35.6	7.0
	0.5	12.4	2.4
	0.5	9.2	1.8
	0.5	11.1	2.2
	0.6	37.7	10.7
	0.6	27.6	7.8
	0.6	19.3	5.5
	0.6	64.7	18.3
	0.6	47.0	13.3
	0.6	32.0	9.0
	0.6	21.4	6.1
	0.6	41.6	11.8
	0.6	46.3	13.1
	0.6	19.4	5.5
	0.7	49.0	18.9
	0.7	29.3	11.3
	0.7	48.2	18.5
	0.7	14.3	5.5
	0.8	53.0	26.6
	0.8	14.6	7.3
	0.8	17.4	8.7
	0.8	29.1	14.6
	0.8	7.6	3.8
	0.8	14.1	7.1
	0.9	60.4	38.4
	0.9	31.6	20.1
	0.9	36.6	23.3
	0.9	8.9	5.7
	1.0	16.7	13.1
	1.0	20.2	15.9
	1.0	11.9	9.3
	1.0	7.2	5.7
	1.1	15.2	14.4

	1.2	62.1	70.2
	1.2	30.8	34.8
	1.2	103.6	117.2
	1.3	16.6	22.0
	1.4	19.4	29.9
	1.4	30.8	47.4
	1.4	17.5	26.9
	1.6	28.1	56.5
	1.7	29.4	66.7
	1.8	14.0	35.6
	2.1	39.3	136.1
	2.4	28.4	128.5
	2.4	14.0	63.3
	2.5	31.3	153.6
	2.5	33.2	163.0
	2.5	12.7	62.3
	2.6	70.4	373.8
	2.7	43.6	249.6
	2.9	29.6	195.5
	3.0	43.8	309.6
	3.0	67.1	474.3
	3.4	76.2	691.8
	4.1	93.0	1250.7

Table B3. Fresh and dry root weights, root volume, and root density by soil pit and layer. Roots were dried at 50°C for at least 8 hours. Root volume was calculated as the layer's root weight divided by average root density (g/cm^3). Root density (cm^3/cm^3) was calculated as root volume divided by soil layer volume (1 m x 1 m x layer thickness).

Soil Pit and Layer	Fresh Root Weight (g)	Dry Root Weight (g)	Calculated Root Volume (cm^3)	Calculated Root Density (cm^3/cm^3)
U-1 Moss	1232	831	2112.7	n/a
U-1 Organic	872	637	1495.4	2.04
U-1 Ae	1056	724	1810.9	4.62
U-1 B1	829	566	1421.6	2.60
U-1 B2	11	4	18.9	0.18
U-2 Moss	1754	883	3007.9	n/a
U-2 Organic	2598	1601	4455.2	5.18
U-2 Ae	208	116	356.7	1.97
U-2 B1	243	152	416.7	2.91
U-3 Moss	1764	1131	3025.0	n/a
U-3 Organic	4505	2581	11717.2	16.11
U-3 Ae	134	107	229.8	2.87
U-3 B1	232	149	397.8	4.97
U-3 B2/B3	19	13	32.6	0.29
D-1 Moss	2367	1616	4059.1	n/a
D-1 Organic	482	310	826.6	0.87
D-1 Ae	65	35	111.5	1.55
D-1 B1	33	21	56.6	0.64
D-2 Moss	894	472	1533.1	n/a
D-2 Organic	2407	2132	8934.2	7.77
D-2 B1	52	29	89.2	1.01
D-3 Moss	355	199	608.8	n/a
D-3 Organic	1553	1122	2663.2	2.22

Appendix C: Tree DBH Surveys

Table C1. Tree number, diameter, and alive/dead status for surveys surrounding upslope soil pits. Each survey was a 7.07 x 7.07 m square, centered on a soil pit. All trees within the survey boundaries were counted. Diameter was calculated as measured D=circumference/π.

Soil Pit	Tree Number	Diameter (cm)	Alive?
U-1	1	11.9	Y
	2	12.1	Y
	3	5.7	Dead
	4	16.9	Y
	5	7.0	Dead
	6	20.1	Y
	7	12.1	Y
	8	8.9	Y
	9	12.7	Y
	10	13.5	Y
	11	5.4	Dead
	12	14.5	Y
	13	7.5	Y
	14	10.2	Y
	15	6.8	Y
	16	16.9	Y
	17	13.7	Dead
	18	16.4	Y
	19	9.2	Y
	20	10.8	Y
	21	12.4	Y
	22	6.5	Dead
	23	7.0	Dead
	24	11.8	Dead
	25	12.1	Y
	26	11.8	Y
	27	14.3	Y
	28	7.0	Y
	29	3.2	Dead
	30	9.1	Y
	31	15.0	Y
	32	5.9	Y
	33	12.4	Y
	34	20.4	Y
	35	10.3	Y
	36	8.0	Y
	37	10.5	Y
U-2	1	16.2	Y
	2	3.5	Y
	3	7.8	Y

Table C2. Tree number, diameter, and alive/dead status for surveys surrounding downslope soil pits. Each survey was a 7.07 x 7.07 m square, centered on a soil pit. All trees within the survey boundaries were counted. Diameter was calculated as measured D=circumference/π.

Soil Pit	Tree Number	Diameter (cm)	Alive?
D-1	1	7.0	Dead
	2	8.9	Y
	3	7.8	Y
	4	3.8	Dead
	5	8.9	Y
	6	7.3	Y
	7	8.0	Y
	8	3.0	Dead
	9	13.1	Y
	10	2.2	Dead
	11	1.4	Y
	12	2.4	Dead
	13	9.1	Y
	14	14.0	Y
	15	16.2	Y
	16	10.5	Y
	17	6.0	Y
	18	2.9	Y
	19	12.1	Y
	20	3.0	Dead
	21	8.1	Y
	22	9.5	Y
	23	1.6	Dead
	24	5.4	Y
	25	3.5	Y
	26	12.7	Y
	27	8.9	Y
	28	12.6	Y
	29	7.0	Y
	30	1.9	Dead
	31	3.7	Dead
	32	8.1	Y
	33	4.5	Dead
	34	7.8	Y
	35	7.0	Y
	36	7.6	Y
	37	12.6	Y
	38	14.5	Y
	39	6.5	Y
	40	9.1	Y
	41	8.9	Y

	4	16.2	Y
	5	5.9	Y
	6	5.4	Y
	7	6.7	Y
	8	17.2	Y
	9	8.6	Dead
	10	15.6	Y
	11	4.5	Y
	12	17.2	Y
	13	11.8	Y
	14	18.8	Y
	15	3.8	Dead
	16	15.6	Y
	17	13.7	Y
	18	15.3	Y
	19	6.7	Dead
	20	14.6	Y
	21	9.5	Y
	22	6.7	Dead
	23	9.7	Y
	24	11.6	Y
	25	19.4	Y
	26	4.5	Dead
	27	6.8	Y
	28	15.0	Y
	29	16.4	Y
	30	10.2	Y
	31	5.3	Y
	32	5.7	Y
	33	5.7	Y
	34	6.4	Y
	35	4.5	Y
	36	7.5	Y
	37	10.8	Y
	38	10.5	Y
	39	4.5	Y
	40	16.6	Y
	41	5.1	Y
	42	3.2	Y
	43	10.8	Y
U-3	1	7.6	Y
	2	8.3	Y
	3	14.3	Y
	4	17.3	Y
	5	3.0	Y
	6	14.3	Y
	7	4.8	Y
	8	13.1	Y
	9	4.1	Dead
	10	8.0	Y
	11	8.0	Y
	12	14.0	Y

	42	9.7	Y
	43	15.1	Y
	44	6.8	Y
	45	7.3	Y
	46	2.9	Y
	47	7.2	Y
	48	5.7	Y
	49	4.0	Y
	50	4.6	Y
	51	13.7	Y
	52	5.6	Dead
	53	14.0	Y
	54	13.7	Y
	55	2.9	Y
	56	11.0	Y
	57	2.2	Dead
	58	10.3	Dead
	59	3.2	Y
	60	4.5	Dead
	61	5.3	Y
	62	3.0	Dead
	63	3.7	Dead
D-2	1	15.0	Y
	2	19.1	Y
	3	7.0	Dead
	4	3.2	Dead
	5	2.1	Dead
	6	16.9	Y
	7	21.5	Y
	8	16.9	Y
	9	11.1	Y
	10	17.5	Y
	11	12.9	Y
	12	6.7	Dead
	13	11.0	Dead
	14	9.2	Y
	15	11.3	Dead
	16	8.6	Dead
	17	15.0	Y
	18	22.0	Y
	19	7.3	Y
	20	14.6	Y
	21	8.4	Y
	22	13.4	Y
	23	7.3	Y
	24	8.3	Dead
	25	12.4	Y
	26	16.1	Y
	27	6.2	Dead
D-3	1	10.8	Y
	2	15.4	Y

	13	8.0	Y
	14	11.3	Y
	15	15.9	Y
	16	12.4	Y
	17	10.0	Y
	18	7.6	Y
	19	6.2	Y
	20	4.1	Y
	21	7.3	Y
	22	6.2	Y
	23	9.5	Y
	24	8.4	Y
	25	2.7	Y
	26	8.6	Y
	27	12.9	Y
	28	11.5	Y
	29	3.3	Dead
	30	16.6	Y
	31	9.9	Y
	32	15.9	Y
	33	13.1	Y
	34	9.4	Y
	35	5.1	Dead
	36	6.8	Dead
	37	7.0	Y
	38	5.4	Dead
	39	20.4	Y
	40	10.8	Y
	41	1.9	Dead
	42	3.0	Y
	43	3.3	Y
	44	5.3	Dead
	45	4.6	Dead
	46	4.3	Y
	47	17.7	Y
	48	11.8	Y
	49	13.7	Y
	50	2.4	Dead
	51	11.1	Y
	52	14.3	Y
	53	5.7	Y
	54	6.8	Y
	55	7.6	Y
	56	3.0	Y

	3	12.1	Y
	4	9.2	Y
	5	7.6	Dead
	6	15.9	Y
	7	13.4	Y
	8	6.5	Y
	9	25.9	Y
	10	8.9	Y
	11	12.4	Y
	12	11.6	Y
	13	3.5	Dead
	14	7.5	Y
	15	5.9	Dead
	16	18.5	Y
	17	16.2	Y
	18	7.2	Dead
	19	2.2	Y
	20	9.5	Y
	21	2.2	Dead
	22	14.0	Y
	23	13.1	Y
	24	10.5	Dead
	25	17.3	Y
	26	16.9	Y
	27	14.3	Y
	28	15.9	Y
	29	8.9	Y
	30	8.3	Y
	31	11.5	Y
	32	16.6	Y
	33	16.9	Y

Appendix D: Microtopography Transects

Table D1. Measurements of relative topography (RT), moss layer thickness, dead moss layer (DM) thickness, and O-horizon thickness along upslope transect.

Distance (m)	RT (cm)	Moss (cm)	DM (cm)	O (cm)
0.0	31	5	5	10
0.25	40.5			
0.5	36.5			
0.75	37.5			
1.0	34	6	10	13
1.25	35			
1.5	40			
1.75	39.5			
2.0	42	6	7	20
2.25	45			
2.5	45			
2.75	45			
3.0	46.5	5	4	4
3.25	45			
3.5	46			
3.75	42			
4.0	44	4	10	3
4.25	48			
4.5	48			
4.75	45			
5.0	42	4	6	14
5.25	39			
5.5	37			
5.75	49			
6.0	48.5	4	8	18
6.25	42			
6.5	39			
6.75	40			
7.0	44	5	7	4
7.25	45			
7.5	43			
7.75	30			
8.0	32	9	5	3
8.25	29			
8.5	29			
8.75	31			
9.0	27	8	12	10
9.25	31			
9.5	32			
9.75	22			
10.0	24	9	7	10
10.25	24			
10.5	28			
10.75	36			
11.0	40	10	6	7

Table D2. Measurements of relative topography (RT), moss layer thickness, dead moss layer (DM) thickness, and O-horizon thickness along downslope transect.

Distance (m)	RT (cm)	Moss (cm)	DM (cm)	O (cm)
0.0		4	2	2
0.25	33			
0.5	32			
0.75	26			
1.0	27.5	3	16	6
1.25	26.5			
1.5	24			
1.75	23			
2.0	26	5	8	11
2.25	26			
2.5	32			
2.75	32.5			
3.0	30.5	6	19	0
3.25	29			
3.5	31.5			
3.75	29			
4.0	25	6	7	13
4.25	18			
4.5	16			
4.75	21			
5.0	15.5	4	10	0
5.25	20.5			
5.5	19			
5.75	11.5			
6.0	11	5	3	9
6.25	10			
6.5	11.5			
6.75	18			
7.0	24	5	7	10
7.25	35.5			
7.5	30			
7.75	26.5			
8.0	26	5	10	8
8.25	30.5			
8.5	33			
8.75	43			
9.0	29	7	12	6
9.25	21			
9.5	13			
9.75	6			
10.0	9	6	17	7
10.25	3			
10.5	15			
10.75	24			
11.0	26	4	5	1

11.25	41			
11.5	35			
11.75	37.5			
12.0	33.5	6	7	6
12.25	41			
12.5	40			
12.75	43			
13.0	45	6	10	8
13.25	43			
13.5	46			
13.75	43			
14.0	41	6	13	7
14.25	46			
14.5	44			
14.75	49			
15.0	40	7	6	5
15.25	29			
15.5	27			
15.75	23			
16.0	38	5	5	4
16.25	49			
16.5	48			
16.75	49			
17.0	46	5	5	5
17.25	40			
17.5	38			
17.75	45.5			
18.0	33	6	11	25
18.25	39			
18.5	39			
18.75	44			
19.0	27	6	14	4
19.25	25			
19.5	26			
19.75	31			
20.0	27	4	8	10
20.25	25			
20.5	26			
20.75	31			
21.0	33	6	7	6
21.25	28			
21.5	20			
21.75	15			
22.0	18	6	4	12
22.25	14			
22.5	17			
22.75	19			
23.0	23	5	10	3
23.25	21.5			
23.5	21			
23.75	18			
24.0	16	5	3	7

11.25	31			
11.5	31			
11.75	40			
12.0	37	4	9	2
12.25	39			
12.5	37			
12.75	44.5			
13.0	37	5	10	4
13.25	28			
13.5	24			
13.75	24.5			
14.0	22	6	11	6
14.25	17			
14.5	43			
14.75	55.5			
15.0	52.5	4.5	6.5	5
15.25	52.5			
15.5	51.5			
15.75	55			
16.0	58	6	10	13
16.25	46.5			
16.5	40			
16.75	35			
17.0	38.5	6	9	11
17.25	45			
17.5	46			
17.75	41			
18.0	40	8	7	15
18.25	36			
18.5	29.5			
18.75	23			
19.0	31.5	5.5	12.5	7
19.25	28			
19.5	32			
19.75	40			
20.0	31	6	6	5
20.25	28			
20.5	25.5			
20.75	23			
21.0		5	9	4
22.0		5	11	6
23.0		5	5	4
24.0		2	6	1

25.0		4	3	3
26.0		5	5	8
27.0		4	14	0
28.0		7	7	19
29.0		6	3	6
30.0		3	5	6
31.0		6	6	11
32.0		5	5	4
33.0		3	10	6
34.0		6	6	12
35.0		6	9	6
36.0		4	9	5

25.0		4	8	6
26.0		3	8	16
27.0		4	9	7
28.0		4	11	10
29.0		4	6	3
30.0		4	10	7
31.0		4	16	3
32.0		5	8	5
33.0		5	5	11

Bibliography

Angstmann, JL, BE Ewers, and H Kwon, 2012, Size-mediated tree transpiration along soil drainage gradients in a boreal black spruce forest wildfire chronosequence: Tree Physiology, v. 32, no. 5, p. 599–611.

Arp, CD, MN Gooseff, MA Baker, and W Wurtsbaugh, 2006, Surface-water hydrodynamics and regimes of a small mountain stream–lake ecosystem: Journal of Hydrology, v. 329, no. 3, p. 500–513.

Athukorala, DN, 2020, The seasonal and inter-annual variation in water export from a boreal forest headwater stream: St. John's, NL, CA, Memorial University of Newfoundland, 196 p.

Billings, SA, D Hirmas, PL Sullivan, CA Lehmeier, S Bagchi, K Min, Z Brecheisen, E Hauser, R Stair, R Flournoy, and D deB Richter, 2018, Loss of deep roots limits biogenic agents of soil development that are only partially restored by decades of forest regeneration: Elementa Science of the Anthropocene, v. 6, no. 1, p. 34.

Bond, BJ, JA Jones, G Moore, N Phillips, D Post, and JJ McDonnell, 2002, The zone of vegetation influence on baseflow revealed by diel patterns of streamflow and vegetation water use in a headwater basin: Hydrological Processes, v. 16, no. 8, p. 1671–1677.

Boronina, A, S Golubev, and W Balderer, 2005, Estimation of actual evapotranspiration from an alluvial aquifer of the Kouris catchment (Cyprus) using continuous streamflow records: Hydrological Processes, v. 19, no. 20, p. 4055–4068.

Bowering, KL, KA Edwards, K Prestegaard, X Zhu, and SE Ziegler, 2020, Dissolved organic carbon mobilized from organic horizons of mature and harvested black spruce plots in a mesic boreal region: Biogeosciences, v. 17, no. 3, p. 581–595.

Brantley, SL, DM Eissenstat, JA Marshall, SE Godsey, Z Balogh-Brunstad, DL Karwan, SA Papuga, J Roering, TE Dawson, J Evaristo, O Chadwick, JJ McDonnell, and KC Weathers, 2017, Reviews and syntheses: on the roles trees play in building and plumbing the critical zone: Biogeosciences, v. 14, no. 22, p. 5115–5142.

D'Orangeville, L, D Houle, L Duchesne, RP Phillips, Y Bergeron, and D Kneeshaw, 2018, Beneficial effects of climate warming on boreal tree growth may be transitory: Nature Communications, v. 9, no. 1, p. 1–10.

Fan, Y, M Clark, DM Lawrence, S Swenson, LE Band, SL Brantley, PD Brooks, WE Dietrich, A Flores, G Grant, JW Kirchner, DS Mackay, JJ McDonnell, PCD Milly, PL Sullivan, C Tague, H Ajami, N Chaney, A Hartmann et al., 2019, Hillslope Hydrology in Global Change Research and Earth System Modeling: Water Resources Research, v. 55, no. 2, p. 1737–1772.

Fan, Y, G Miguez-Macho, EG Jobbágy, RB Jackson, and C Otero-Casal, 2017, Hydrologic regulation of plant rooting depth: Proceedings of the National Academy of Sciences, v. 114, no. 40, p. 10572–10577.

von Freyberg, J, B Studer, M Rinderer, and JW Kirchner, 2018, Studying catchment storm response using event- and pre-event-water volumes as fractions of precipitation rather than discharge: Hydrology and Earth System Sciences, v. 22, no. 11, p. 5847–5865.

Graly, J, J Harrington, and N Humphrey, 2017, Combined diurnal variations of discharge and hydrochemistry of the Isunnguata Sermia outlet, Greenland Ice Sheet: The Cryosphere, v. 11, no. 3, p. 1131–1140.

Gribovszki, Z, P Kalicz, J Szilágyi, and M Kucsara, 2008, Riparian zone evapotranspiration estimation from diurnal groundwater level fluctuations: Journal of Hydrology, v. 349, no. 1, p. 6–17.

Gribovszki, Z, J Szilágyi, and P Kalicz, 2010, Diurnal fluctuations in shallow groundwater levels and streamflow rates and their interpretation – A review: Journal of Hydrology, v. 385, no. 1, p. 371–383.

Gurnell, AM, and CR Fenn, 1985, Spatial and Temporal Variations in Electrical Conductivity in a Pro-Glacial Stream System: Journal of Glaciology, v. 31, no. 108.

Jackson, RB, J Canadell, JR Ehleringer, HA Mooney, OE Sala, and ED Schulze, 1996, A global analysis of root distributions for terrestrial biomes: Oecologia, v. 108, no. 3, p. 389–411.

Jencso, KG, BL McGlynn, MN Gooseff, SM Wondzell, KE Bencala, and LA Marshall, 2009, Hydrologic connectivity between landscapes and streams: Transferring reach- and plot-scale understanding to the catchment scale: Water Resources Research, v. 45, no. 4.

Knapp, JLA, J von Freyberg, B Studer, L Kiewiet, and JW Kirchner, 2020, Concentration-discharge relationships vary among hydrological events, reflecting differences in event characteristics: Hydrology and Earth System Sciences Discussions, p. 1–27.

Leach, JA, W Lidberg, L Kuglerová, A Peralta-Tapia, A Ågren, and H Laudon, 2017, Evaluating topography-based predictions of shallow lateral groundwater discharge zones for a boreal lake-stream system: Water Resources Research, v. 53, no. 7, p. 5420–5437.

Lehmann, J, and M Kleber, 2015, The contentious nature of soil organic matter: Nature, v. 528, no. 7580, p. 60–68.

Maeght, J-L, B Rewald, and A Pierret, 2013, How to study deep roots—and why it matters: Frontiers in Plant Science, v. 4.

Moroni, M, P Carter, and D Ryan, 2009, Harvesting and slash piling affect soil respiration, soil temperature, and soil moisture regimes in Newfoundland boreal forests: Canadian Journal of Soil Science, v. 89, p. 343-355.

Morris, DA, and AI Johnson, 1967, Summary of hydrologic and physical properties of rock and soil materials, as analyzed by the hydrologic laboratory of the U.S. Geological Survey, 1948-60, USGS Numbered Series 1839-D: U.S. Government Printing Office, Water Supply Paper.

Mutzner, R, SV Weijs, P Tarolli, M Calaf, HJ Oldroyd, and MB Parlange, 2015, Controls on the diurnal streamflow cycles in two subbasins of an alpine headwater catchment: Water Resources Research, v. 51, no. 5, p. 3403–3418.

Pierret, A, and G Lacombe, 2018, Hydrologic regulation of plant rooting depth: Breakthrough or observational conundrum? Proceedings of the National Academy of Sciences, v. 115, no. 12, p. E2669–E2670.

Pulliainen J, M Aurela, T Laurila, T Aalto, M Takala, M Salminen, M Kulmala, A Barr, M Heimann, A Lindroth, A Laaksonen, C Derksen, A Mäkelä, T Markkanen, J Lemmetyinen, J Susiluoto, S Dengel, I Mammarella, JP Tuovinen, and T Vesala, 2017, Early snowmelt significantly enhances boreal springtime carbon uptake: Proceedings of the National Academy of Sciences, v. 114, no. 42, p. 11081–11086.

Pierret, A, J-L Maeght, C Clément, J-P Montoroi, C Hartmann, and S Gonkhamdee, 2016, Understanding deep roots and their functions in ecosystems: an advocacy for more unconventional research: Annals of Botany, v. 118, no. 4, p. 621–635.

Reich, PB, KM Sendall, A Stefanski, RL Rich, SE Hobbie, and RA Montgomery, 2018, Effects of climate warming on photosynthesis in boreal tree species depend on soil moisture: Nature, v. 562, no. 7726, p. 263.

Scharlemann, JP, EV Tanner, R Hiederer, and V Kapos, 2014, Global soil carbon: understanding and managing the largest terrestrial carbon pool: Carbon Management, v. 5, no. 1, p. 81–91.

Senar OE, KL Webster KL, and IF Creed, 2018, Catchment-scale shifts in the magnitude and partitioning of carbon export in response to changing hydrologic connectivity in a northern hardwood forest. Journal of Geophysical Research: Biogeosciences, v. 123, no. 8, p. 2337–2352.

Simmons, D, 2019, Determining the Accuracy of Remotely-Sensed Evapotranspiration Estimates for Boreal Forest Ecosystems: College Park, MD, USA, University of Maryland, 75 p.

Tranvik LJ, JA Downing, JB Cotner, SA Loiselle, RG Striegl, TJ Ballatore, P Dillon, K Finlay, K Fortino, LB Knoll, PL Kortelainen, T Kutser, S Larsen, I Laurion, DM Leech, SL McCallister, DM McKnight, JM Melack, E Overholt, JA Porter, Y Prairie, WH Renwick, F Roland, BS Sherman, DW Schindler, S Sobek, A Tremblay, MJ Vanni, AM Verschoor, E von Wachenfeldt, and GA Weyhenmeyer, 2009, Lakes and reservoirs as regulators of carbon cycling and climate: Limnology and Oceanography, v. 54, no. 6, p. 2298–2314.

Trenberth, KE, L Smith, T Qian, A Dai, and J Fasullo, 2007, Estimates of the Global Water Budget and Its Annual Cycle Using Observational and Model Data: Journal of Hydrometeorology, v. 8, no. 4, p. 758–769.

Ulrich, W, B Kusumoto, T Shiono, and Y Kubota, 2016, Climatic and geographic correlates of global forest tree species–abundance distributions and community evenness: Journal of Vegetation Science, v. 27, no. 2, p. 295–305.

Wang, Y, EH Hogg, DT Price, J Edwards, and T Williamson, 2014, Past and projected future changes in moisture conditions in the Canadian boreal forest: The Forestry Chronicle, v. 90, no. 5, p. 678–691.

Wetzel, RG, 2001, Limnology: Lake and River Ecosystems: Gulf Professional Publishing, 1023 p.

Ziegler, SE, R Benner, SA Billings, KA Edwards, M Philben, X Zhu, and J Laganière, 2017, Climate Warming Can Accelerate Carbon Fluxes without Changing Soil Carbon Stocks: Frontiers in Earth Science, v. 5.